A theory of particle deposition in turbulent pipe flow

By JOHN YOUNG and ANGUS LEEMING

Whittle Laboratory, University of Cambridge, Madingley Road, Cambridge, CB3 0DY, UK

The paper describes a theory of particle deposition based formally on the conservation equations of particle mass and momentum. These equations are formulated in an Eulerian coordinate system and are then Reynolds averaged, a procedure which generates a number of turbulence correlations, two of which are of prime importance. One represents 'turbulent diffusion' and the other 'turbophoresis', a convective drift of particles down gradients of mean-square fluctuating velocity. Turbophoresis is not a small correction; it dominates the particle dynamic behaviour in the diffusion-impaction and inertia-moderated regimes.

Adopting a simple model for the turbophoretic force, the theory is used to calculate deposition from fully developed turbulent pipe flow. Agreement with experimental measurements is good. It is found that the Saffman lift force plays an important role in the inertia-moderated regime but that the effect of gravity on deposition from vertical flows is negligible. The model also predicts an increase in particle concentration close to the wall in the diffusion-impaction regime, a result which is partially corroborated by an independent 'direct numerical simulation' study.

The new deposition theory represents a considerable advance in physical understanding over previous free-flight theories. It also offers many avenues for future development, particularly in the simultaneous calculation of laminar (pure inertial) and turbulent particle transport in more complex two- and three-dimensional geometries.

1. Introduction

The problem of predicting the deposition rate of small particles suspended in a turbulent gas flow in a pipe has occupied the attention of researchers for more than forty years. Work has undoubtedly been stimulated by its practical relevance to many areas of technology and science but interest has also been aroused by the intellectual challenge of the problem and the inability of any theory to provide a truly satisfying physical explanation of the observed facts.

These facts are well-known and are not in dispute. They are also quite dramatic. Figure 1 summarizes the content of many experiments of which the most frequently quoted are those of Liu & Agarwal (1974). The figure shows the rate of particle deposition on the wall of a circular pipe as a function of particle size, the variables being non-dimensionalized in the conventional fashion. Thus, the dimensionless deposition velocity V_{dep+} is defined by

$$V_{dep+} = \frac{J_w}{\rho_{pm} u_*},\tag{1}$$

where J_w is the mass flux of particles to the wall per unit area, ρ_{pm} is the mean particle
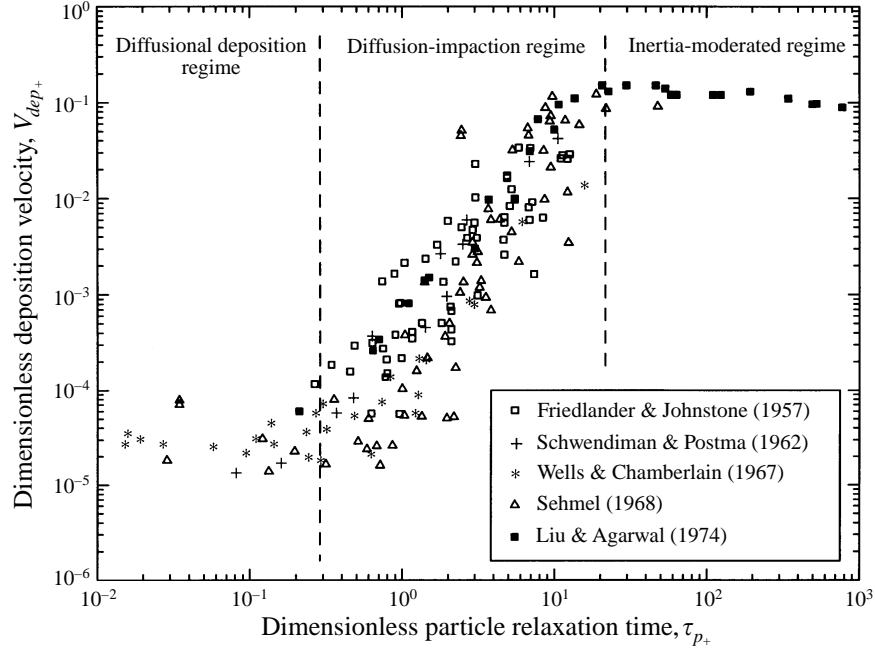
FIGURE 1. Particle deposition from fully developed turbulent pipe flow: a summary of experimental data.

density in the pipe (mass of particles per unit volume) and u_* is the friction velocity ($u_*^2 = \tau_w/\rho_g$, where τ_w is the wall shear stress and ρ_g is the gas density). The dimensionless particle relaxation time τ_{p+} is defined by

$$\tau_{p+} = \tau_p u_*^2/\nu_g, \tag{2}$$

where ν_g is the kinematic viscosity of the gas. τ_p is the particle relaxation time,

$$\tau_p = \frac{\rho_{mat} d_p^2}{18 \rho_g \nu_g}(1 + 2.7Kn), \tag{3}$$

where d_p is the particle diameter, ρ_{mat} is the particle material density and $Kn = \lambda_g/d_p$ is the particle Knudsen number, λ_g being the mean free path of a gas molecule. The expression for τ_p is based on the Stokes drag law for a spherical particle modified by a correction factor $(1 + 2.7Kn)$ due to Cunningham (1910) which models deviations from continuum behaviour when the particle diameter is comparable with the molecular mean free path.

The deposition curves of figure 1 are nominally divided into three regimes. In the 'diffusional deposition' regime, V_{dep+} is a monotonically decreasing function of τ_{p+} and also depends on the particle Schmidt number, $Sc = \nu_g/D_p$, where D_p is the particle Brownian diffusion coefficient. D_p is assumed to be given by the Einstein equation,

$$D_p = R_p T \tau_p, \tag{4}$$

T being the temperature (the flow is assumed to be isothermal), and $R_p = k/m_p$, where k is Boltzmann's constant and $m_p = \pi d_p^3 \rho_{max}/6$ is the mass of a particle. In this regime, particle transport to the wall is well represented by a gradient diffusion model, that is by 'turbulent diffusion' in the core of the pipe and Brownian diffusion in a very thin layer directly adjacent to the wall.

In the 'diffusion-impaction' regime, a dramatic increase in deposition rate of several orders of magnitude is observed corresponding to about a fourfold increase in particle diameter. From the early days, this was recognized, quite correctly, as the result of the interaction between particles having significant inertia and the fluid turbulent eddies. Starting from the work of Friedlander & Johnstone (1957), a theory, variously referred to as the 'free-flight' or 'stop-distance' model, was developed over a period of more than twenty years. The essence of the model is that particles are transported by gradient diffusion to within one 'stop-distance' of the wall where they acquire sufficient inertia to 'coast' across the viscous sub-layer.

The free-flight model lacks rigour but it does provide an attractive physical explanation with the exception of one, very serious, shortcoming. In order to obtain agreement with experiment, it is necessary to assume that the particles acquire a velocity towards the wall at the stop distance approximately equal to the friction velocity u_*. However, at these locations of between about 1 and 10 'wall units' from the surface (one wall unit corresponds to a distance v_g/u_*), the r.m.s. fluctuating velocity of the gas is very much less than u_* and it has never been satisfactorily explained how the particles acquire the necessary wallwards momentum from the prevailing low level of turbulence. Indeed, a more formally correct interpretation of the free-flight model (Davies 1966) predicts deposition rates some two orders of magnitude less than those observed experimentally.

The third region is known as the 'inertia-moderated' regime. Here, gradient diffusion is assumed to play little or no part, the very massive particles acquiring sufficient momentum from the large eddies in the turbulent core to reach the wall directly. The reduction in deposition rate with increasing particle size is explained by the fact that the increasing particle inertia results in a decreasing response to the turbulence.

Many variations of the stop-distance model can be found in the literature and the reader is referred to the review by Papavergos & Hedley (1984) for details. However, virtually all analyses are based on matching a solution of the particle conservation equation (derived under an assumption of equal particle and gas time-mean velocities) to a free-flight model at an interface located one stop-distance from the wall. The momentum equation for the particles is generally not invoked despite the fact that this provides the only possibility for estimating the particle convective velocity generated by the fluid turbulence, i.e. the phenomenon accepted as being responsible for the huge increase in deposition rate in the diffusion-impaction regime.

Recently, however, two important papers have examined the role of the momentum equation in the deposition process. By using a Monte Carlo method based on Lagrangian 'particle tracking' in a numerically generated random flow field, Kallio & Reeks (1989) were able to demonstrate the main features of the deposition curves shown in figure 1. Johansen (1991) also found good agreement with experiment by adopting a fully Eulerian approach with empirical closure models for the particle turbulence terms.

This paper proposes a more formal theory of deposition in fully developed isothermal turbulent pipe flow. The governing equations are formulated in an Eulerian framework and are then Reynolds averaged. This helps to clarify the physical processes responsible for deposition and also highlights ways of extending the model to more complex flow fields than the pipe flow considered here. Johansen (1991) chose to work with the equations in divergence-free form but this has the disadvantage of obscuring the dominating physical processes by the proliferation of turbulence terms. A more transparent analysis results from the use of the equations in non-conservative form.

Consideration is also given to the wall boundary conditions. To date, scant attention has been paid to their correct form, despite their importance to deposition. Accordingly, a new, physically based, model boundary condition for the particle density is proposed.

2. The particle equations of motion

Consider the flow of small particles suspended in a gas. The particles are assumed to be spherical and monodispersed of diameter d_p and mass m_p. If the number of particles per unit volume is n_p, then the particle density (mass per unit volume) is $\rho_p = n_p m_p$. (ρ_p should not be confused with ρ_{mat} the material density of the particles.) The analysis is restricted to dilute suspensions of particles, implying that the fluid motion is unaffected by the presence of the particles and that particle–particle collisions are unimportant. The conditions for which these assumptions are valid are discussed by Johansen (1991) and are fulfilled for most reported experiments on particle deposition from turbulent gas flows.

The equations describing particle motion in a gas are the conservation equations of particle mass (or number) and momentum. The effect of the gas in controlling the motion enters via the momentum equation in providing 'external' force terms acting on the particles. These external fluid force terms must be specified in some way before a solution to the particle equations can be found. For a complex three-dimensional turbulent gas flow field no general approach to this very difficult problem exists but, for the simple pipe flow considered here, sufficiently accurate models of the turbulence are available.

Let J be a vector representing the total mass flux of particles per unit area. The 'total' particle velocity V_T is then defined by the equality

$$J = \rho_p V_T. \tag{5}$$

V_T is a mean velocity averaged over the random thermal motions of all the particles which are treated, in this respect, as large molecules. Conservation of mass for the particles is then expressed in differential form by the equation

$$\frac{\partial \rho_p}{\partial t} + \nabla \cdot (\rho_p V_T) = 0. \tag{6}$$

It should be noted that the mass flux due to Brownian diffusion does not appear explicitly in (6) when written in terms of V_T (Fernandez de la Mora & Rosner 1982).

The particle momentum equation is given by (Ramshaw 1979, 1981)

$$\rho_p \left[\frac{\partial V_T}{\partial t} + (V_T \cdot \nabla) V_T \right] = -\nabla p_p + \rho_p F + \rho_p g, \tag{7}$$

where p_p is the partial pressure associated with the random thermal motion of the particles, F is the force exerted by the gas on the particles per unit mass of particles (averaged over the random thermal motions) and g is the acceleration due to gravity. Electrostatic forces have been neglected but could be introduced if desired. (Note that, when taking the divergence of the particle stress tensor to obtain the term $-\nabla p_p$, the particle 'viscous' stresses have also been neglected.)

In evaluating p_p it is assumed that the particles and gas are in thermal equilibrium. Equipartition of energy then requires

$$p_p = n_p kT = \rho_p R_p T, \tag{8}$$

and hence, assuming the flow is isothermal,

$$\nabla p_p = R_p T \nabla \rho_p = \frac{D_p}{\tau_p} \nabla \rho_p, \tag{9}$$

where D_p is the particle Brownian diffusion coefficient given by (4). Strictly speaking, the substitution of (9) into (7) is only valid when the left-hand side of (7) is negligible compared to $-\nabla p_p$. However, the only time when Brownian diffusion is important as a particle transport mechanism is for very small particles extremely close to the wall and this is precisely when the left-hand side of (7) becomes negligibly small compared with $-\nabla p_p$. In other situations, the calculated value of the Brownian flux will be in error, but this flux will be totally overshadowed by other transport mechanisms.

As discussed in detail by Maxey & Riley (1983), the force F exerted by the fluid on the particles includes contributions from the steady-state viscous drag, the Basset force, the virtual mass effect, the force due to the fluid pressure gradient, the Saffman lift force due to fluid shear, the Magnus force due to particle rotation and the thermophoretic force (if the flow is non-isothermal). In principle, these can all be included in the analysis but when $\rho_{mat} \gg \rho_g$ (a condition assumed here) the only significant contributions in isothermal flow are from the steady-state viscous drag F_D and, possibly, the Saffman lift force F_L. Hence,

$$F = F_D + F_L. \tag{10}$$

The steady-state viscous drag per unit particle mass is given by

$$F_D = \frac{\Phi_D}{\tau_p}(U - V_T), \tag{11}$$

where U is the gas velocity and τ_p is the particle relaxation time given by equation (3). Φ_D is a function of the particle slip Reynolds number ($Re_p = d_p|U - V_T|/\nu_g$) and is given by

$$\Phi_D = \frac{Re_p}{24} C_D, \tag{12}$$

where $C_D = C_D(Re_p)$ is the particle drag coefficient. Values of C_D were obtained from the empirical representation of Morsi & Alexander (1972). For pipe flow, the Saffman lift force acts in the radial direction and is given (per unit particle mass) by

$$F_L = \text{sign}(\kappa)\, 3.08 \Phi_L \rho_g \rho_{mat}^{-1} \nu_g^{1/2} d_p^{-1}(U_z - V_z)|\kappa|^{1/2} e_r = F_L e_r, \tag{13}$$

where $\kappa = \partial U_z/\partial r$ is the shear rate (z and r are the axial and radial coordinates respectively), e_r is a unit vector in the radial direction and $\Phi_L = \Phi_L(Re_p)$ is an empirical correction due to Mei (1992) to account for the effects of finite particle slip Reynolds numbers. For the usual situation in pipe flow where the particles lead the gas near the wall, $\kappa < 0$, $V_z > U_z$ and the Saffman force is directed towards the pipe wall thus tending to enhance the deposition rate.

According to Fischer & Rosenberger (1987) and McLaughlin (1993), the drag and lift forces should be modified when the particles are very close to the wall. Although these corrections could be integrated into (11) and (13), they have not been included in order to avoid confusion. The modifications are unlikely to affect the overall deposition rate but could influence the particle concentration profiles very near the wall.

Substituting (9), (10) and (11) into the momentum equation (7) gives

$$\left[\frac{\partial V_T}{\partial t} + (V_T \cdot \nabla) V_T\right] = -\frac{D_p}{\tau_p \rho_p}\nabla \rho_p + \frac{\Phi_D}{\tau_p}(U - V_T) + F_L + g. \tag{14}$$

The total mass flux of particles J is now represented as the sum of a convective and a Brownian diffusive contribution,

$$J = J_{conv} + J_{diff}, \tag{15}$$

where $J_{diff} = -D_p \nabla \rho_p$ by definition. Writing $J_{conv} = \rho_p V$, equation (15) serves to define the particle convective velocity V,

$$\rho_p V_T = \rho_p V - D_p \nabla \rho_p. \tag{16}$$

Combining (6) and (16) gives the more familiar form of the particle mass conservation equation

$$\frac{\partial \rho_p}{\partial t} + \nabla \cdot (\rho_p V) = \nabla \cdot (D_p \nabla \rho_p). \tag{17}$$

Substituting (16) in (14) then gives for the momentum equation

$$\left[\frac{\partial V}{\partial t} + (V \cdot \nabla) V \right] = \frac{\Phi_D}{\tau_p} (U - V) + F_L + g, \tag{18}$$

where V_T has been replaced by V in the acceleration term. This is justifiable because, in those regions of the flow where Brownian diffusion is insignificant $V \approx V_T$, and in those regions where Brownian diffusion dominates the acceleration term is negligible anyway.

Equations (17) and (18) form the basis for the development of the deposition theory described below. In passing, however, it is instructive to consider how the usual methods of solution for inertial deposition (Lagrangian tracking) and diffusional deposition (Eulerian integration) arose. The momentum equation (18) may be written

$$\frac{\mathrm{D} V}{\mathrm{D} t} = \frac{\Phi_D}{\tau_p} (U - V) + F_L + g, \tag{19}$$

where $\mathrm{D}/\mathrm{D}t$ is the substantive derivative following a particle. This equation in Lagrangian form does not involve ρ_p and can be solved for V if the gas velocity field U is known. Conversely, when diffusion is the dominant transport mechanism, the particle conservation equation (17) for steady flow in Eulerian form is

$$\nabla \cdot (\rho_p V - D_p \nabla \rho_p) = 0. \tag{20}$$

This can be solved for ρ_p without recourse to (19) if it is assumed that $V = U$ and is known. The success of the present method is largely due to the fact that both equations are retained and solved simultaneously.

3. The Reynolds-averaged equations

For steady vertical pipe flow in a cylindrical polar coordinate system (r, ϕ, z) with z measured vertically downwards, (17) and (18) take the following form (neglecting Brownian diffusion in the axial direction):

$$\frac{1}{r} \frac{\partial}{\partial r} (r \rho_p V_r) + \frac{1}{r} \frac{\partial}{\partial \phi} (\rho_p V_\phi) + \frac{\partial}{\partial z} (\rho_p V_z) = \frac{1}{r} \frac{\partial}{\partial r} \left[r D_p \frac{\partial \rho_p}{\partial r} \right], \tag{21}$$

$$V_r \frac{\partial V_r}{\partial r} + \frac{V_\phi}{r} \frac{\partial V_r}{\partial \phi} + V_z \frac{\partial V_r}{\partial z} - \frac{V_\phi V_\phi}{r} = \frac{\Phi_D}{\tau_p} (U_r - V_r) + F_L, \tag{22}$$

$$V_r \frac{\partial V_z}{\partial r} + \frac{V_\phi}{r} \frac{\partial V_z}{\partial \phi} + V_z \frac{\partial V_z}{\partial z} = \frac{\Phi_D}{\tau_p} (U_z - V_z) + g. \tag{23}$$

The ϕ-component of the momentum equation has been omitted because it yields no useful information for axisymmetric flow. The Saffman force F_L is defined by (13).

For turbulent flow, time-mean and fluctuating components are introduced in the usual way by

$$\rho_p = \bar{\rho}_p + \rho'_p,$$

$$V_r = \bar{V}_r + v'_r, \quad U_r = \bar{U}_r + u'_r,$$

$$V_\phi = \bar{V}_\phi + v'_\phi, \quad U_\phi = \bar{U}_\phi + u'_\phi,$$

$$V_z = \bar{V}_z + v'_z, \quad U_z = \bar{U}_z + u'_z,$$

where, for fully developed pipe flow, $\bar{U}_r = 0$.

The flow is assumed to be axisymmetric so that the circumferential variation of all time-mean quantities (including products of fluctuating quantities) is zero. The flow is also assumed to be non-swirling and hence $\bar{V}_\phi = \bar{U}_\phi = 0$. At this stage, it is not intrinsically obvious that a fully developed turbulent particle flow in a pipe is physically attainable but, in anticipation of later results, the assumption will be made that the time-mean particle velocity field is independent of the axial coordinate, i.e. $\partial \bar{V}_r / \partial z = \partial \bar{V}_z / \partial z = 0$. $\partial \bar{\rho}_p / \partial z$ is not zero, however, as the particle density decreases in the flow direction due to the deposition on the walls of the pipe. The axial variation of the time-mean of all products of fluctuating components is also assumed to be zero.

The Reynolds-averaged particle mass and momentum equations are thus

$$\frac{1}{r}\frac{\partial}{\partial r}(r\bar{\rho}_p \bar{V}_r) + \frac{\partial}{\partial z}(\bar{\rho}_p \bar{V}_z) = \frac{1}{r}\frac{\partial}{\partial r}\left[rD_p\frac{\partial \bar{\rho}_p}{\partial r}\right] - \frac{1}{r}\frac{\partial}{\partial r}(r\overline{\rho'_p v'_r}), \tag{24}$$

$$\bar{V}_r\frac{\partial \bar{V}_r}{\partial r} = -\frac{\bar{\Phi}_D \bar{V}_r}{\tau_p} + \bar{F}_L + \frac{\overline{v'_\phi v'_\phi}}{r} - \overline{(\boldsymbol{v}'\cdot\boldsymbol{\nabla})v'_r}, \tag{25}$$

$$\bar{V}_r\frac{\partial \bar{V}_z}{\partial r} = \frac{\bar{\Phi}_D(\bar{U}_z - \bar{V}_z)}{\tau_p} + g - \overline{(\boldsymbol{v}'\cdot\boldsymbol{\nabla})v'_z}, \tag{26}$$

where $\boldsymbol{v}'$ is a vector having components (v'_r, v'_ϕ, v'_z) in cylindrical polar coordinates and contributions to $\bar{F}_L$ from the velocity fluctuations are ignored. The final terms in (25) and (26) can be simplified by introducing the particle mass conservation equation (neglecting the contribution from Brownian diffusion). Thus,

$$\overline{(\boldsymbol{v}'\cdot\boldsymbol{\nabla})v'_r} = \overline{\boldsymbol{\nabla}\cdot(v'_r\boldsymbol{v}')} - \overline{v'_r(\boldsymbol{\nabla}\cdot\boldsymbol{v}')} = \overline{\boldsymbol{\nabla}\cdot(v'_r\boldsymbol{v}')} + \overline{v'_r\boldsymbol{V}\cdot\boldsymbol{\nabla}(\ln\rho_p)},$$

$$\overline{(\boldsymbol{v}'\cdot\boldsymbol{\nabla})v'_z} = \overline{\boldsymbol{\nabla}\cdot(v'_z\boldsymbol{v}')} - \overline{v'_z(\boldsymbol{\nabla}\cdot\boldsymbol{v}')} = \overline{\boldsymbol{\nabla}\cdot(v'_z\boldsymbol{v}')} + \overline{v'_z\boldsymbol{V}\cdot\boldsymbol{\nabla}(\ln\rho_p)}.$$

Hence,

$$\bar{V}_r\frac{\partial \bar{V}_r}{\partial r} = -\frac{\bar{\Phi}_D \bar{V}_r}{\tau_p} + \bar{F}_L - \frac{\partial}{\partial r}\overline{(v'_r v'_r)} + \frac{\overline{(v'_\phi v'_\phi - v'_r v'_r)}}{r} - \overline{v'_r\boldsymbol{V}\cdot\boldsymbol{\nabla}(\ln\rho_p)}, \tag{27}$$

$$\bar{V}_r\frac{\partial \bar{V}_z}{\partial r} = \frac{\bar{\Phi}_D(\bar{U}_z - \bar{V}_z)}{\tau_p} + g - \frac{\partial}{\partial r}\overline{(v'_r v'_z)} - \frac{\overline{(v'_r v'_z)}}{r} - \overline{v'_z\boldsymbol{V}\cdot\boldsymbol{\nabla}(\ln\rho_p)}. \tag{28}$$

Equations (24), (27) and (28) are the basic equations describing time-mean particle transport in turbulent non-swirling pipe flow. With the exception of the work of Johansen (1991), previous analyses have been confined to equation (24) alone with the mandatory assumption that $\bar{V}_r = \bar{U}_r = 0$ and $\bar{V}_z = \bar{U}_z$ (there being no other method of

calculating the mean particle slip velocity). This is a serious deficiency of any deposition theory because (apart from very small particles) particle transport is dominated in certain regions of the pipe, not by diffusive, but by convective effects. (The 'stop-distance' theory can actually be viewed as a crude attempt to confront this problem by dividing the flow field into an outer diffusive region where (24) is operative and an inner region close to the wall where convective effects (specified in a very arbitrary way) dominate.)

4. Turbulence modelling

In order to close the system of equations, it is necessary to specify suitable expressions for the terms involving the fluctuation correlations. Considerable interest is currently being shown in this very difficult problem as exemplified by the work of Reeks (1993) who, in a series of papers, is attempting to derive the constitutive equations of turbulent particle flow from a fundamental kinetic equation similar to the Boltzmann equation in the kinetic theory of gases. The aims of the present study, however, are rather to demonstrate that the basic physical processes involved in particle deposition can be quantitatively represented using comparatively simple theoretical models.

Accordingly, the term $\overline{(\rho_p' v_r')}$ in (24) is modelled by 'gradient diffusion',

$$-\overline{(\rho_p' v_r')} = D_{turb} \frac{\partial \bar{\rho}_p}{\partial r}, \tag{29}$$

where D_{turb} is the particle turbulent diffusion coefficient. D_{turb} is related to the fluid turbulent kinematic viscosity ν_{turb} by the turbulent Schmidt number,

$$Sc_{turb} = \nu_{turb}/D_{turb}. \tag{30}$$

For very small particles, Sc_{turb} is expected to be near unity in analogy with the turbulent Prandtl number. For larger particles displaying inertia effects, theories of particle dispersion in *homogeneous isotropic* turbulence also indicate a turbulent Schmidt number close to 1. In physical terms, although larger particles respond less well to the turbulent fluctuations of the fluid, their velocities are more persistent, with the net effect that dispersion remains approximately independent of particle size. This conclusion emerged from Tchen's original analysis (see Hinze 1975, Sections 5–7) and has been confirmed by later work (Reeks 1977; Pismen & Nir 1978).

Problems arise, however, when there is significant particle drift due to strong inhomogeneities in the turbulence. In such cases, particles entrained by eddies in one region of the flow acquire sufficient inertia to drift into regions with quite different turbulence characteristics while still retaining a 'memory' of their earlier motion. Various attempts have been made to adjust the value of D_{turb} in these circumstances (Liu & Ilori 1974; Picart, Berlemont & Gouesbet 1986) but in reality the modifications represent little more than empirical tuning to provide better agreement with experimental data. The real problem centres on the attempt to represent experimental measurements of particle dispersion in complex turbulent flows by a single correlation of the form of equation (29). In contrast, the model proposed here assumes that the term $-\overline{(\rho_p' v_r')}$ is unaltered from its value in homogeneous isotropic turbulence (i.e. an assumption of 'local equilibrium') and that convective particle drift arises from a quite different physical effect, the source of which is the dominant turbulence term in the radial momentum equation.

Accordingly, because the current level of knowledge is insufficient to justify a more elaborate model, it is assumed that the turbulent Schmidt number is everywhere unity. Equation (24) expressing the conservation of particle mass is therefore written

$$\frac{1}{r}\frac{\partial}{\partial r}(r\bar{\rho}_p \bar{V}_r) + \frac{\partial}{\partial z}(\bar{\rho}_p \bar{V}_z) = \frac{1}{r}\frac{\partial}{\partial r}\left[r(D_p + D_{turb})\frac{\partial\bar{\rho}_p}{\partial r}\right], \tag{31}$$

with D_{turb} given by (30) with $Sc_{turb} = 1$. The specification of the gas eddy viscosity ν_{turb} (which is assumed known) is discussed below.

The dominant turbulence correlation in the radial momentum equation (27) is $-\partial\overline{(v'_r v'_r)}/\partial r$, a term which represents the tendency of particles to acquire a drift velocity in the direction of decreasing turbulence intensity. The effect has been graphically termed 'turbophoresis' (Reeks 1983) and is the cause of the huge increase in deposition rate in the eddy-impaction regime. Physically, particles in regions of high turbulence intensity acquire comparatively large fluctuating components of velocity enabling them to drift into regions where the turbulence level is insufficiently high to supply them with the necessary momentum for the return journey. In some respects, therefore, the free-flight theory of deposition can be viewed as an intuitive but crude attempt to model the term $-\partial\overline{(v'_r v'_r)}/\partial r$.

Accurate representation of the turbophoretic term is difficult because, due to particle drift, the radial component of the mean-square fluctuating velocity of the particles $\overline{(v'_r v'_r)}$ may not relate directly to the *local* radial component of the mean-square fluctuating velocity of the gas $\overline{(u'_r u'_r)}$, which is assumed known. For the present, however, this 'memory effect' of the particles is ignored and the assumption is made that $\overline{(v'_r v'_r)}$ depends only on the *local* value of $\overline{(u'_r u'_r)}$ just as if the particles were in equilibrium in a homogeneous isotropic turbulence field. Thus,

$$-\frac{\partial}{\partial r}\overline{(v'_r v'_r)} = -\frac{\partial}{\partial r}[\Gamma\overline{(u'_r u'_r)}], \tag{32}$$

where $\Gamma = \overline{(v'_r v'_r)}/\overline{(u'_r u'_r)}$ is a function of τ_p and the local persistance time of the turbulent eddies τ_g. Theories of particle dispersion (Reeks 1977) indicate the relationship

$$\Gamma \approx \frac{\tau_g}{\tau_g + \tau_p}. \tag{33}$$

The eddy timescale τ_g is difficult to specify precisely being equivalent neither to the Eulerian nor to the Lagrangian integral timescales. It is defined here by the relationship

$$\nu_{turb} = \overline{(u'_r u'_r)}\tau_g. \tag{34}$$

Like ν_{turb}, $\overline{(u'_r u'_r)}$ is assumed known and its specification is discussed below.

The term $\overline{(v'_\phi v'_\phi - v'_r v'_r)}/r$ in (27) is neglected because it is only appreciable very near the centre of the pipe and therefore has little effect on deposition. The final term $\overline{v'_r V}\cdot\nabla(\ln\rho_p)$ would be zero if the particle field were incompressible (which it is not). Large gradients of ρ_p do not occur simultaneously with large convection velocities, however, and it is unlikely that this term plays a significant role in particle transport. It is thus evident that the dominant turbulence term in (27) is the turbophoretic term. Accordingly, the working form of the radial momentum equation is

$$\bar{V}_r\frac{\partial\bar{V}_r}{\partial r} = -\frac{\bar{\Phi}_D \bar{V}_r}{\tau_p} - \frac{\partial}{\partial r}[\Gamma\overline{(u'_r u'_r)}] + \bar{F}_L. \tag{35}$$

Assuming for the moment that the effect of the Saffman force is of secondary importance, (35) shows very clearly that the mean acceleration of the particles towards the wall originates from the gradient of the fluid turbulence intensity (the turbophoretic force) and is opposed by the mean viscous drag of the fluid.

If the Saffman force is neglected, the deposition rate can be obtained by solving (35) for $\bar{V}_r$ followed by (31) for $\bar{\rho}_p$ without recourse to the axial momentum equation. Inclusion of the Saffman force couples the two momentum equations, however, because the axial slip velocity $(\bar{U}_z - \bar{V}_z)$ is needed to evaluate $\bar{F}_L$, see (13). Adopting similar arguments as for the radial momentum equation, the final two terms in (28) are neglected, giving the working form of the axial momentum equation as

$$\bar{V}_r \frac{\partial \bar{V}_z}{\partial r} = \frac{\bar{\Phi}_D(\bar{U}_z - \bar{V}_z)}{\tau_p} - \frac{\partial}{\partial r}\overline{(v_r' v_z')} + g. \tag{36}$$

This equation is less important than the radial momentum equation and the modelling of the turbulence term $-\overline{(v_r' v_z')}$ is not crucial. Accordingly, it is represented by a gradient diffusion model with turbulent kinematic viscosity equal to that of the background gas,

$$-\overline{(v_r' v_z')} = \nu_{turb} \frac{\partial \bar{V}_z}{\partial r}. \tag{37}$$

5. Boundary conditions

In seeking solutions to (31), (35) and (36), it is of prime importance to specify the boundary conditions correctly. In previous theories, this aspect of the problem has been seriously neglected. Here, only the simplest case of a perfectly absorbing wall is considered. Particle reflection is not allowed.

The radial and axial momentum equations are essentially convection equations for $\bar{V}_r$ and $\bar{V}_z$. The influence of the pipe wall is therefore not transmitted upstream along the time-mean particle trajectories and it is only necessary to specify conditions at the centre-line, $r = 0$ (denoted below by subscript 0). These conditions are

$$\bar{V}_{r0} = 0, \tag{38}$$

$$\bar{V}_{z0} = \bar{U}_{z0} + g\tau_p/\bar{\Phi}_{D0}. \tag{39}$$

The particle mass conservation equation is a convection–diffusion equation and, as such, the wall exerts an upstream influence upon the particle flow. It therefore requires boundary conditions at both the centreline and the pipe wall. At the centreline, flow symmetry considerations dictate that

$$\left(\frac{\partial \bar{\rho}_p}{\partial r}\right)_0 = 0. \tag{40}$$

At the pipe wall (which is assumed to be perfectly absorbing), the commonly applied boundary condition for particle density is $\bar{\rho}_p = 0$ but this is only (approximately) correct for the limiting case of very small particles transported to the wall by Brownian diffusion with zero convective velocity (Lee, Hanratty & Adrian 1989). In some respects, the situation is similar to that of a vapour diffusing through a carrier gas and condensing at a cooled surface. For problems of this type, the boundary condition cannot be specified in purely continuum terms but must be established from a kinetic

analysis of the particle behaviour very close to the absorbing surface. A new model boundary condition has therefore been developed and details of the theory are presented in Appendix A. The final equation is

$$J_w = \left[\bar{\rho}_p \bar{V}_r - (D_p + D_{turb}) \frac{\partial \bar{\rho}_p}{\partial r} \right]_w$$

$$= \left[\tfrac{1}{2} \bar{\rho}_p \bar{V}_r \left(1 + \mathrm{erf}(M_r) + \frac{1}{\pi^{1/2} M_r} \exp(-M_r^2) \right) \right]_w, \tag{41}$$

where J is the particle mass flux, $M_r = \bar{V}_r/(2R_p T)^{1/2}$ is a dimensionless time-mean particle convective velocity, $R_p = k/m_p$, erf is the error function and subscript w indicates that all terms are to be evaluated at the wall (or, more strictly, at one particle radius from the wall).

It is instructive to consider the behaviour of (41) for two limiting cases. First, when the convective mass flux at the wall dominates over the Brownian diffusive flux, $M_{rw} \to \infty$, $\mathrm{erf}(M_{rw}) \to 1$, $\exp(-M_{rw}^2) \to 0$, and the boundary condition becomes

$$\left(\frac{\partial \bar{\rho}_p}{\partial r} \right)_w = 0, \tag{42}$$

expressing the physical fact that the wall exerts no upstream influence on the particle flow. Secondly, when the Brownian flux dominates, $M_{rw} \to 0$, $\mathrm{erf}(M_{rw}) \to 0$, $\exp(-M_{rw}^2) \to 1$, and the boundary condition becomes

$$-(D_p + D_{turb}) \left(\frac{\partial \bar{\rho}_p}{\partial r} \right)_w = \bar{\rho}_{pw} \left(\frac{R_p T}{2\pi} \right)^{1/2}, \tag{43}$$

an expression (familiar from the kinetic theory of gases) relating the diffusive flux to the rate at which particles are projected towards the wall.

From (43), valid for the diffusive limit, it is evident that, in order to maintain a concentration gradient at the wall, $\bar{\rho}_{pw}$ cannot be precisely zero. The commonly applied boundary condition of $\bar{\rho}_{pw} = 0$ is therefore strictly incorrect even in diffusion-dominated deposition processes. In convection-dominated processes, $\bar{\rho}_{pw}$ is of similar magnitude to the centreline value $\bar{\rho}_{p0}$.

6. Fully developed particle flow in pipes

The term 'fully developed particle flow' implies that, in some sense to be determined, the particle velocity and density profiles are independent of the axial location. It is not intuitively obvious that such a particle flow is physically attainable and the governing equations and boundary conditions must therefore be re-examined in order to express them in a form independent of z.

The radial and axial momentum equations (35) and (36) can be written in dimensionless form as

$$V_{r+} \frac{\mathrm{d}\bar{V}_{r+}}{\mathrm{d}r_+} = -\frac{\bar{\Phi}_D \bar{V}_{r+}}{\tau_{p+}} - \frac{\mathrm{d}}{\mathrm{d}r_+} [\Gamma \overline{(u'_{r+} u'_{r+})}] + \bar{F}_{L+}, \tag{44}$$

$$V_{r+} \frac{\mathrm{d}\bar{V}_{z+}}{\mathrm{d}r_+} = \frac{\bar{\Phi}_D (\bar{U}_{z+} - \bar{V}_{z+})}{\tau_{p+}} - \frac{\mathrm{d}}{\mathrm{d}r_+} \overline{(v'_{r+} v'_{z+})} + g_+, \tag{45}$$

Schematic of mean-square fluctuating
particle velocity profile

Time-mean particle trajectories
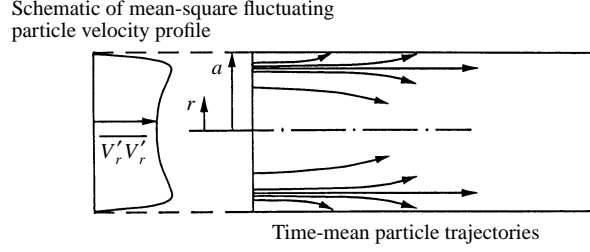
FIGURE 2. Hypothetical particle movement in a turbulent pipe flow due to turbophoresis alone.

subject to the boundary conditions

$$(\bar{V}_{r+})_0 = 0, \tag{46}$$

$$(\bar{V}_{z+})_0 = (\bar{U}_{z+})_0 + g_+ \tau_{p+}/\bar{\Phi}_{D0}. \tag{47}$$

In these equations, $r_+ = ru_*/\nu_g$, $\tau_{p+} = \tau_p u_*^2/\nu_g$, $g_+ = g\nu_g/u_*^3$, $\bar{F}_{L+} = \bar{F}_L \nu_g/u_*^3$ and all velocities are non-dimensionalized with respect to u_*. Total, as opposed to partial, derivatives have been used in anticipation of the following remarks.

Neglecting the Saffman force, (44) and (46) provide a complete specification for $\bar{V}_{r+}$ which is independent of z. The turbulence terms depend mainly on r_+ (and to a much lesser extent on the dimensionless pipe radius $a_+ = au_*/\nu_g$) and hence

$$\bar{V}_{r+} = \bar{V}_{r+}(r_+, a_+, \tau_{p+}). \tag{48}$$

Similarly,
$$\bar{V}_{z+} = \bar{V}_{z+}(r_+, a_+, \tau_{p+}, g_+). \tag{49}$$

For given a_+, τ_{p+} and g_+, the dimensionless particle time-mean velocity field is identical at all axial locations once the fully developed steady state has been established. Inclusion of the Saffman force couples the two equations but does not alter this conclusion.

At this point, it is interesting to consider the effect of the turbophoretic term in (44). As shown in figure 2, the radial variation of $\overline{(u_r' u_r')}$ is such that, for $y_+ = a_+ - r_+ < 40$, the effect of turbophoresis is to propel particles towards the wall while, for $y_+ > 40$, particles are projected (rather less forcibly because of the gentler gradient) towards the pipe centreline. A fully developed particle flow independent of z can therefore only be maintained if the effects of turbulent particle diffusion are such as to counteract exactly the changes in the particle density profile brought about by the influence of turbophoresis. This is one role of the diffusive terms in the particle conservation equation.

Because of deposition on the pipe wall, $\bar{\rho}_p = \bar{\rho}_p(r, z)$. A dimensionless time-mean particle density $\bar{\psi}$ is now defined by the relationship

$$\bar{\psi} = \frac{\bar{\rho}_p(r, z)}{\bar{\rho}_{pm}(z)}, \quad \bar{\rho}_{pm}(z) = \frac{2}{a^2} \int_0^a r\bar{\rho}_p(r, z) \, \mathrm{d}r. \tag{50}$$

$\bar{\rho}_{pm}(z)$ is the time-mean particle density averaged across the pipe (the 'pipe-mean' particle density) and is a function of z only. It will now be shown that $\bar{\psi}$ is a function of r only.

Consider first the variation of $\bar{\rho}_{pm}$ with z. Assuming for the present that $\bar{\psi} = \bar{\psi}(r)$, the mass flux to the wall is

$$J_w(z) = \bar{\rho}_{pm}(z)\left[\bar{\psi}\bar{V}_r - (D_p + D_{turb})\frac{\mathrm{d}\bar{\psi}}{\mathrm{d}r}\right]_w. \tag{51}$$

A deposition velocity is now defined by $V_{dep} = J_w(z)/\bar{\rho}_{pm}(z)$ and is given in dimensionless form by

$$V_{dep+} = \frac{V_{dep}}{u_*} = \left[\bar{\psi}\bar{V}_{r+} - \left(\frac{1}{Sc} + \frac{1}{Sc_{turb}}\frac{\nu_{turb}}{\nu_g}\right)\frac{\mathrm{d}\bar{\psi}}{\mathrm{d}r_+}\right]_w. \tag{52}$$

It therefore follows that, if $\bar{\psi} = \bar{\psi}(r)$, V_{dep+} is independent of z. The total particle mass flow rate at any axial location is

$$M_p(z) = \int_0^a 2\pi r \bar{\rho}_p(r, z)\,\bar{V}_z(r)\,\mathrm{d}r = \bar{\rho}_{pm}(z)\int_0^a 2\pi r\bar{\psi}(r)\,\bar{V}_z(r)\,\mathrm{d}r, \tag{53}$$

where a is the pipe radius and $\bar{\psi} = \bar{\psi}(r)$ has again been assumed. A dimensionless particle mass flow rate, independent of z, is thus given by

$$M_{p+} = \frac{M_p(z)\,u_*}{\bar{\rho}_{pm}(z)\,\nu_g^2} = \int_0^{a_+} 2\pi r_+\,\bar{\psi}(r_+)\,\bar{V}_z(r_+)\,\mathrm{d}r_+. \tag{54}$$

Global conservation of particle mass requires

$$\frac{\mathrm{d}M_p(z)}{\mathrm{d}z} = -2\pi a J_w(z). \tag{55}$$

Substituting (51) and (53) into (55) and introducing (52) and (54) gives

$$\frac{\mathrm{d}\bar{\rho}_{pm}(z_+)}{\mathrm{d}z_+} = -K\bar{\rho}_{pm}(z_+), \tag{56}$$

where $K = 2\pi a V_{dep+}/M_{p+} = \text{constant}$. Hence, if $\bar{\psi} = \bar{\psi}(r)$, the pipe-mean particle density decays exponentially according to

$$\bar{\rho}_{pm}(z_+) = \bar{\rho}_{pm}(0)\exp(-Kz_+), \tag{57}$$

where $\bar{\rho}_{pm}(0)$ is the value of $\bar{\rho}_{pm}$ at $z = z_+ = 0$.

Non-dimensionalizing the particle mass conservation equation (31) with respect to the wall variables and introducing (56) results in

$$\frac{1}{r_+}\frac{\mathrm{d}}{\mathrm{d}r_+}(r_+\bar{\psi}\bar{V}_{r+}) - K\bar{\psi}\bar{V}_{z+} = \frac{1}{r_+}\frac{\mathrm{d}}{\mathrm{d}r_+}\left[r_+\left(\frac{1}{Sc} + \frac{1}{Sc_{turb}}\frac{\nu_{turb}}{\nu_g}\right)\frac{\mathrm{d}\bar{\psi}}{\mathrm{d}r_+}\right], \tag{58}$$

an equation which is independent of z. Similar non-dimensionalization of the boundary conditions, (40) and (41), gives

$$\left(\frac{\mathrm{d}\bar{\psi}}{\mathrm{d}r_+}\right)_0 = 0, \tag{59}$$

$$V_{dep+} = \left[\bar{\psi}\bar{V}_{r+} - \left(\frac{1}{Sc} + \frac{1}{Sc_{turb}}\frac{\nu_{turb}}{\nu_g}\right)\frac{\mathrm{d}\bar{\psi}}{\mathrm{d}r_+}\right]_w$$

$$= \left[\tfrac{1}{2}\bar{\psi}\bar{V}_{r+}\left(1 + \mathrm{erf}(M_r) + \frac{1}{\pi^{1/2}M_r}\exp(-M_r^2)\right)\right]_w, \tag{60}$$

which are also independent of z. It has therefore been shown that the scaling defined by (50) results in a set of dimensionless equations which are completely independent of z and therefore representative of fully developed turbulent particle flow in pipes.

7. Solution of the particle equations

The complete set of particle equations in dimensionless form comprises the radial and axial momentum equations (44) and (45) together with their boundary conditions (46) and (47), and the particle conservation equation (58) with its boundary conditions (59) and (60). The equations do not yield an analytical solution but are readily solved numerically using a 'time-marching' approach. To this end, a time-derivative term is added to each of (44), (45) and (58). Also, in anticipation of later discussion, the radial coordinate r_+ is replaced by $y_+ = a_+ - r_+$, the dimensionless distance from the wall. Hence,

$$\frac{\partial \bar{V}_{y+}}{\partial t_+} = -\bar{V}_{y+} \frac{\partial \bar{V}_{y+}}{\partial y_+} + \frac{\bar{\Phi}_D \bar{V}_{y+}}{\tau_{p+}} - \frac{\partial}{\partial y_+}[\Gamma \overline{(u'_{y+} u'_{y+})}] + \bar{F}_{L+}, \tag{61}$$

$$\frac{\partial \bar{V}_{z+}}{\partial t_+} = -\bar{V}_{y+} \frac{\partial \bar{V}_{z+}}{\partial y_+} + \frac{\bar{\Phi}_D (\bar{U}_{z+} - \bar{V}_{z+})}{\tau_{p+}} - \frac{\partial}{\partial y_+}(\overline{v'_{y+} v'_{z+}}) + g_+, \tag{62}$$

$$\frac{\partial \bar{\psi}}{\partial t_+} = -\frac{1}{r_+} \frac{\partial}{\partial y_+}(r_+ \bar{\psi} \bar{V}_{y+}) + K \bar{\psi} \bar{V}_{z+} + \frac{1}{r_+} \frac{\partial}{\partial y_+}\left[r_+ \left(\frac{1}{Sc} + \frac{1}{Sc_{turb}} \frac{\nu_{turb}}{\nu_g}\right) \frac{\partial \bar{\psi}}{\partial y_+}\right], \tag{63}$$

where $t_+ = t u_*^2 / \nu_g$. The three unknown (dimensionless) dependent variables are the wall-normal and axial time-mean convective velocities $\bar{V}_{y+}$ and $\bar{V}_{z+}$, and the time-mean particle density $\bar{\psi}$. All turbulence quantities are known if the wall-normal variations of the gas eddy viscosity ν_{turb}, the turbulent Schmidt number Sc_{turb} and the mean-square fluctuating gas velocity $(\overline{u'_{y+} u'_{y+}})$ are specified. The gas axial velocity profile $\bar{U}_{z+}(y_+)$ can be obtained by solving the Navier–Stokes equations with the specified variation of ν_{turb}. After discretization, the solution of the equations is obtained by marching forward in 'time' from an arbitrary initial condition until a steady state corresponding to $\partial/\partial t_+ = 0$ is attained.

By introducing the particle *convective* velocity (as opposed to the *total* velocity, see (16)) and by using the 'non-conservative' form of the radial and axial momentum equations, $\bar{\psi}$ has been eliminated completely from (61) and (62). These may therefore be solved for $\bar{V}_{y+}$ and $\bar{V}_{z+}$ in advance of solving for $\bar{\psi}$ using (63). Numerical conservation of momentum cannot, of course, be guaranteed using a non-conservative differencing scheme but then neither is it a physically realistic requirement: an unbalanced source of momentum already exists due to the assumption of a one-way coupling between the gas and particle phases. However, having determined $\bar{V}_{y+}$ and $\bar{V}_{z+}$, the solution for $\bar{\psi}$ may then be accomplished using a fully conservative finite volume technique, ensuring that spurious numerical creation or loss of particles does not occur.

The domain of integration extends from the wall to the pipe centreline and, because of the rapidly varying turbulence, it is expedient to use a non-uniform (but smoothly varying) discretization with the finest spacing near the wall. The situation is most critical for small particles which respond very rapidly to the changing gas turbulence. The behaviour of larger particles is more muted and, in consequence, the grid spacing can be coarser. These changing requirements can be met in practice for the momentum equations by setting the increment adjacent to the wall equal to one particle radius and then increasing the spacing towards the pipe centreline according to a suitable geometric progression.

The particle radial and axial velocity fields are obtained by a semi-implicit time-marching integration of (61) and (62). The derivatives $\partial/\partial t_+$ and $\partial/\partial y_+$ are replaced by

forward time and central space finite difference approximations respectively. The equations are then marched forward in time until the steady-state solution is reached. Because the equations are of the pure convection type, a small amount of second-order artificial viscosity must be added to provide the necessary upwinding for numerical stability. It is also desirable to represent the steady-state drag terms implicitly for otherwise the maximum time step for numerical stability is of the same order as the particle relaxation time and this results in large computational times for very small particles. All other spatial derivatives are expressed explicitly, however.

The particle conservation equation is solved on a different computational grid. In the limit of purely diffusional transport, the deposition rate is controlled by the particle density gradient at the wall and, when Brownian diffusion dominates, this can be very steep indeed. The grid spacing adjacent to the wall is therefore established automatically by the computer program in such a way that the change in $\bar{\psi}$ across the first increment is no greater than 0.05. The remainder of the grid is again defined by a (different) geometric progression and both the gas and particle velocity fields are interpolated onto it using a spline interpolation routine. The solution of the particle conservation equation is then obtained using a conservative implicit finite volume time-marching scheme. Details of the numerical discretization and the implementation of the boundary conditions can be found in Leeming (1996).

8. Specification of the gas turbulence

The theory of particle deposition described above assumes a detailed knowledge of the gas flow field in which the particles are suspended. Differences between predicted and observed deposition rates arise from limitations in both the gas turbulence representation and the particle transport model and it is only possible to validate the latter if the error associated with the former is small. Luckily, the gas turbulence information required for predicting deposition in fully developed pipe flow is minimal. Indeed, it is <u>only</u> necessary to know the radial variations of ν_{turb}, Sc_{turb} (here assumed unity) and $(\overline{u'_y u'_y})$.

Nevertheless, it is still important to specify these quantities accurately. This is particularly true in the near-wall region ($y_+ < 5$) and also in the buffer layer ($5 < y_+ < 40$). The dominant transport mechanism for very small particles is diffusion and the particle flux towards the wall depends on the effective diffusion coefficient ($D_p + D_{turb}$). Even the smallest particles are large and heavy in comparison with gas molecules, however, and the laminar Schmidt number ν_g/D_p rarely falls much below 10^3. The 'laminar' sub-layer for particle diffusion is thus very much thinner than that for momentum transport and so it is necessary to have an accurate model for ν_{turb} much closer to the wall than is required for momentum transport calculations. On the other hand, the transport of larger particles is dominated by inertial effects, the turbophoretic force being dependent on the gradient of $(\overline{v'_y v'_y}) = \Gamma(\overline{u'_y u'_y})$. This is zero at the wall, attains its maximum value in the buffer region at about $y_+ = 20$ and decays to zero again by $y_+ = 40$.

The modelling of both turbulence quantities is also constrained by the stability requirements of the particle transport scheme. The turbophoretic force per unit particle mass is $-\partial[(\overline{v'_y v'_y})]/\partial y$ and, if this is to have a smooth radial variation, it should be continuously differentiable. This in turn requires that $(\overline{v'_y v'_y})$ be twice differentiable, a restriction which also applies to ν_{turb} and $(\overline{u'_y u'_y})$ since $(\overline{v'_y v'_y})$ is a simple function of both through (33) and (34).

The chosen empirical models fulfil all these criteria and are described in detail in
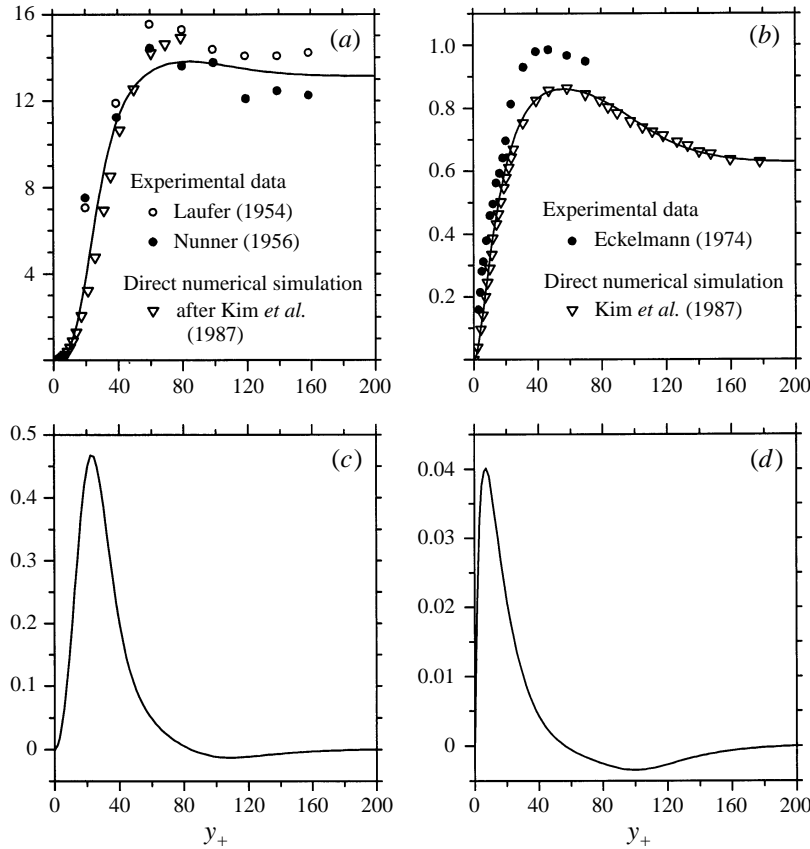
FIGURE 3. Radial variations of (a) ν_{turb}/ν_g and (b) $\overline{(u'_{y+} u'_{y+})}^{1/2}$ and their gradients, (c) and (d) respectively, in fully developed turbulent pipe flow.

Appendix B. Figure 3 shows the variations with y_+ of ν_{turb} and $\overline{(u'_{y+} u'_{y+})}^{1/2}$ and their gradients and also includes a comparison with the experimental measurements of Laufer (1954), Nunner (1956) and Eckelmann (1974) and results from the direct numerical simulation (DNS) of Kim, Moin & Moser (1987).

9. Validation of the particle turbulence models

Modern optical techniques such as particle image velocimetry (PIV) provide a wealth of information about time-mean velocity profiles and turbulence statistics and recent years have seen the publication of a number of experimental studies of particle movement in turbulent flows using this technique. To date, however, PIV has only been applied successfully to liquid flows transporting large (100 μm) particles and the information it provides is of little relevance to the present study. (The particle diameter is comparable to the size of the dominant near-wall eddies and transport by turbophoresis is suppressed.)

Nevertheless, although direct experimental validation of the particle turbulence models is currently not possible, some corroboratory evidence is available from a recent direct numerical simulation (DNS) by Brooke, Hanratty & McLaughlin (1994) of the transport of fine aerosol particles in air in a fully developed channel flow. They investigated three classes of particle having dimensionless diameters d_{p+} of 0.28, 0.36
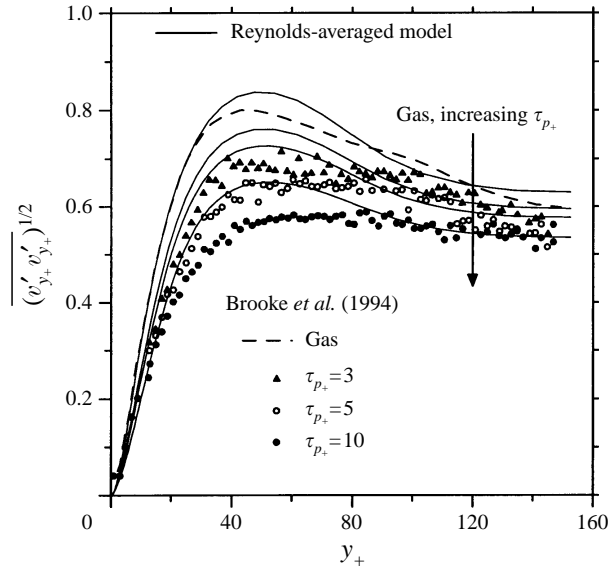
FIGURE 4. Wall-normal r.m.s. fluctuating velocity of gas and particles: a comparison with the direct numerical simulation data of Brooke *et al.* (1994). The arrow crosses the profiles of first the gas and then the three particle classes.

and 0.50, corresponding relaxation times τ_{p+} of 3, 5, and 10, and a material-to-gas density ratio of 713. The channel half-width was 150 wall units and the Reynolds number was 4000. Particles of this size are small enough to interact fully with the eddy structure of the turbulence and their dynamic behaviour is representative of the diffusion–impaction deposition regime.

Figure 4 shows a comparison between the models adopted for the present work and data extracted from the paper by Brooke *et al.* Considering first the variation of $(\overline{u'_{y+} u'_{y+}})^{1/2}$ for the gas, it can be seen that the profile from Brooke *et al.* is rather different from the model described in Appendix B. This is surprising as the latter is a very close fit to the data of Kim *et al.* (1987). Encouragingly, however, the two curves coalesce near the wall and are indistinguishable for $y_+ < 30$, the most important region from the point of view of particle deposition. The variations of $(\overline{v'_{y+} v'_{y+}})^{1/2}$ for the three particle classes were calculated from (3), (33) and (34) and, comparing with the data of Brooke *et al.*, it is evident that the simple theory accurately predicts the dynamic response in the central region of the pipe where the turbulence is near-homogeneous. But even in the strongly inhomogeneous flow closer to the wall, it can be seen that the theory still provides quite a good model. If a discrepancy exists at all, then it is only close to the wall where it is just possible to discern a slight 'memory effect' in the profile for the largest particles ($\tau_{p+} = 10$) as they drift down the turbulence gradient.

Brooke *et al.* also presented results showing the variation of Sc_{turb} across the pipe. The values obtained were in the range $0.6 < Sc_{turb} < 1.4$, a result which lends credence to the assumption of $Sc_{turb} = 1$ adopted for the present work.

10. The effect of turbophoresis

Before discussing the calculations of deposition rate obtained by solution of the full set of equations, it is instructive to consider the effect of turbophoresis in isolation as the role of this very important transport mechanism has not previously been clarified.
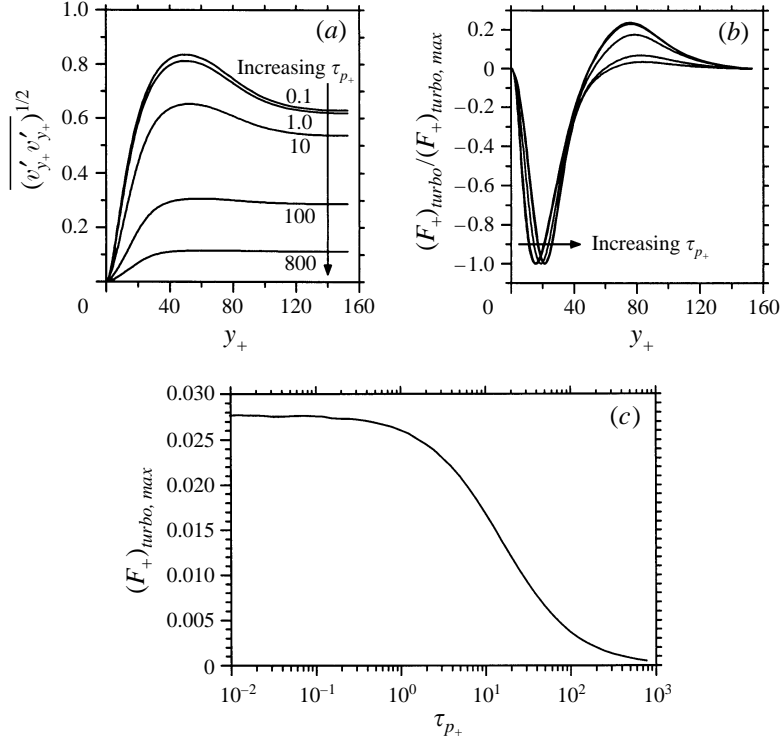
FIGURE 5. Details of the turbophoretic force: (a) Variation of $\overline{(v'_{y+} v'_{y+})}^{1/2}$ with y_+ for various values of τ_{p+}. (b) Corresponding turbophoretic forces scaled by their maximum values. (c) Variation of the maximum turbophoretic force with τ_{p+}.

Figure 5(a) shows the variation of $\overline{(v'_{y+} v'_{y+})}^{1/2}$ with y_+ for selected values of τ_{p+}, calculated using the model described above. Figure 5(b) shows the corresponding dimensionless turbophoretic 'force',

$$(F_+)_{turbo} = -\frac{\mathrm{d}}{\mathrm{d}y_+}(\overline{v'_{y+} v'_{y+}}), \qquad (64)$$

scaled by its own maximum value $(F_+)_{turbo, max}$ which occurs at about $y_+ = 20$, almost independently of τ_{p+}. The variation of $(F_+)_{turbo, max}$ with τ_{p+} is plotted in figure 5(c).

The turbophoretic force accelerates the particles towards the wall creating a convective or 'drift' velocity which is opposed by the viscous drag force. Were the particle acceleration and Saffman force negligible, (61) could easily be solved for $\bar{V}_{y+}$, which might then be appropriately termed the (dimensionless) 'turbophoretic velocity',

$$(\bar{V}_{y+})_{turbo} = -\frac{\tau_{p+}}{\bar{\Phi}_D}\frac{\mathrm{d}}{\mathrm{d}y_+}(\overline{v'_{y+} v'_{y+}}). \qquad (65)$$

Assuming $\bar{\Phi}_D \approx 1$, the maximum value of $(\bar{V}_{y+})_{turbo}$ for a given τ_{p+} occurs at the position of maximum turbophoretic force at $y_+ \approx 20$. The variation of $(\bar{V}_{y+})_{turbo, max}$ with τ_{p+} is thus obtained by multiplying the ordinate of figure 5(c) by τ_{p+}, the result being shown in figure 6. The resemblance of this curve to the experimentally determined dimensionless deposition velocity V_{dep+} (defined by equation (1) and also shown in the figure) is striking and it is worth considering the implications a little further.
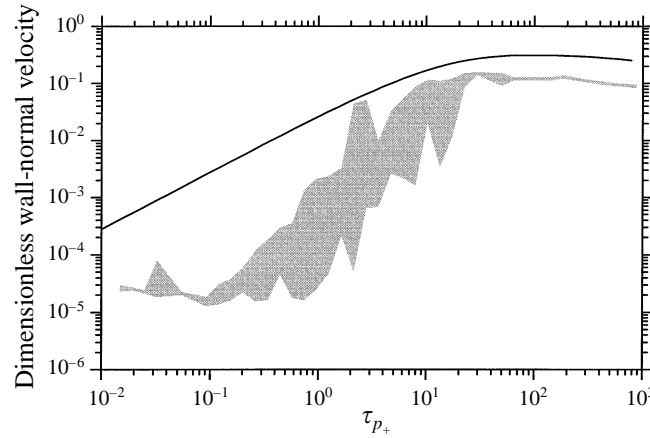
FIGURE 6. Variation of the maximum dimensionless turbophoretic velocity (at $y_+ \approx 20$) with τ_{p+}. Experimental measurements of dimensionless deposition velocity from figure 1 shown for comparison as the shaded region.

Figure 5(c) shows that, for particles with small inertia ($\tau_{p+} < 1$, say), $(F_+)_{turbo, max}$ is almost constant (because $\overline{(v'_{y+} v'_{y+})} \approx \overline{(u'_{y+} u'_{y+})}$). $(\bar{V}_{y+})_{turbo, max}$ is therefore directly proportional to τ_{p+} and hence, as shown in figure 6, tends to zero linearly with τ_{p+}. Physically, particles with small inertia cannot sustain a significant drift velocity against the decelerating influence of viscous drag. Particle inertia increases with increasing τ_{p+}, however, and so $(\bar{V}_{y+})_{turbo, max}$ also increases reaching a flat peak of about 0.3 at $\tau_{p+} \approx 50$. Thereafter, the effect of increasing particle inertia in reducing $\overline{(v'_{y+} v'_{y+})}$ below $\overline{(u'_{y+} u'_{y+})}$ tends to reduce the turbophoretic velocity (although, for the values of τ_{p+} shown in figure 6, the effect is not very pronounced). In this regime, particles with high inertia respond less well to the turbulent fluctuations and so the turbophoretic velocity begins to decline.

When comparing the curves of $(\bar{V}_{y+})_{turbo, max}$ and V_{dep+} in figure 6, it is important to appreciate that the former occurs at $y_+ \approx 20$ whereas the latter is evaluated at the wall itself. The stopping distance s of a particle with relaxation time τ_p given an initial velocity $(\bar{V}_{y+})_{turbo, max}$ is, in dimensionless form, $s_+ = \tau_{p+}(\bar{V}_{y+})_{turbo, max}$. It is therefore only the larger particles ($\tau_{p+} > 50$, say) which have sufficient inertia to coast freely to the wall from $y_+ \approx 20$ and, if the experimentally observed deposition velocities for smaller particles are to be reproduced theoretically, transport mechanisms other than turbophoresis must be operative in the region $y_+ < 20$.

At first glance therefore it might appear that the present theory offers no advantage over the free-flight theory of Davies (1966) (which predicts deposition rates some two orders of magnitude below the experimental values in the diffusion-impaction regime) but this is actually not the case. The present theory provides a formal physical-mathematical explanation of the origin of the force causing a wallwards drift of particles in the buffer layer and shows that this force is proportional to the *gradient* of $\overline{(v'_{y+} v'_{y+})}$. The fact that the impulse supplied by the turbophoretic force is insufficient to propel particles with $\tau_{p+} < 50$ directly to the wall should not be taken as an indication that these particles are incapable of reaching the wall. As will emerge shortly, diffusional transport mechanisms assume dominance when the turbophoretic force declines in order to maintain an almost constant particle flux through the region $y_+ < 20$.
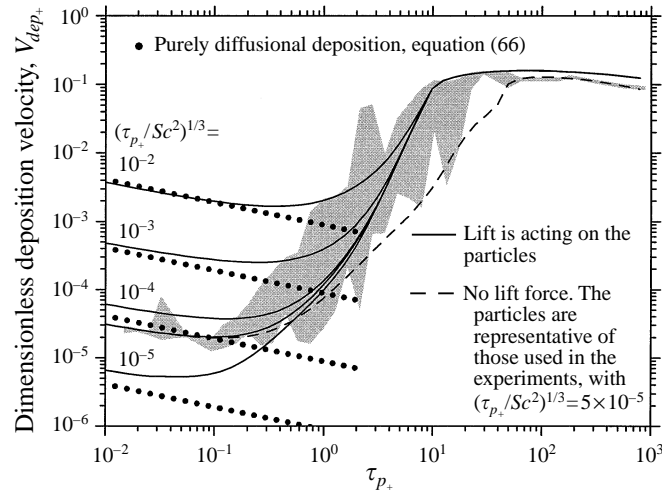
FIGURE 7. Theoretical predictions and experimental measurements (shaded region) of dimensionless deposition velocity.

11. Computed deposition rates and experimental comparison

Figure 7 shows the dimensionless deposition velocity V_{dep+} as a function of τ_{p+} for all three deposition regimes. The various curves were obtained by numerical solution of the complete set of particle equations and should be compared with the compilation of experimental results which is also included in the figure. Clearly, the predictions (particularly when the Saffman force is included) are in excellent agreement with the experimental data. Given the simplicity of the turbulence modelling, this must be classed as a major achievement of the theory.

It can be seen from figure 7 that deposition in the diffusion-impaction and inertia-moderated regimes is dominated by particle inertia and that V_{dep+} is essentially a function of τ_{p+} only. For very small particles, however, the dominant transport mechanism is diffusion. These particles are transported into the sub-layer by turbulent diffusion and finally to the wall by Brownian diffusion, both processes being driven by the particle density gradient. The deposition velocity in this regime, if presented as a function of τ_{p+} is then found to depend on the similarity parameter $(\tau_{p+}/Sc^2)^{1/3}$. This is easily shown analytically by assuming the particle convective velocity to be zero and integrating the particle conservation equation (58) (with $K = 0$) across the sub-layer subject to the known variation of v_{turb}. The integration is similar to that performed by Beal (1970) and gives

$$V_{dep+} = 0.073 Sc^{-2/3} = 0.073 (\tau_{p+}/Sc^2)^{1/3} \tau_{p+}^{-1/3}. \tag{66}$$

The parameter $(\tau_{p+}/Sc^2)^{1/3}$ is independent of particle size if rarefied gas effects are neglected. Figure 7 shows a comparison, for various values of $(\tau_{p+}/Sc^2)^{1/3}$, between (66) and the full numerical solution. Obviously, the latter approaches the correct diffusional limit asymptotically.

12. Interpretation of the particle dynamic behaviour

Apart from providing a simple model for predicting deposition rates in turbulent pipe flow, the theory also furnishes information about the spatial variation of the time-mean particle density and velocities in the pipe and the way in which particles of different sizes respond to the turbulence.
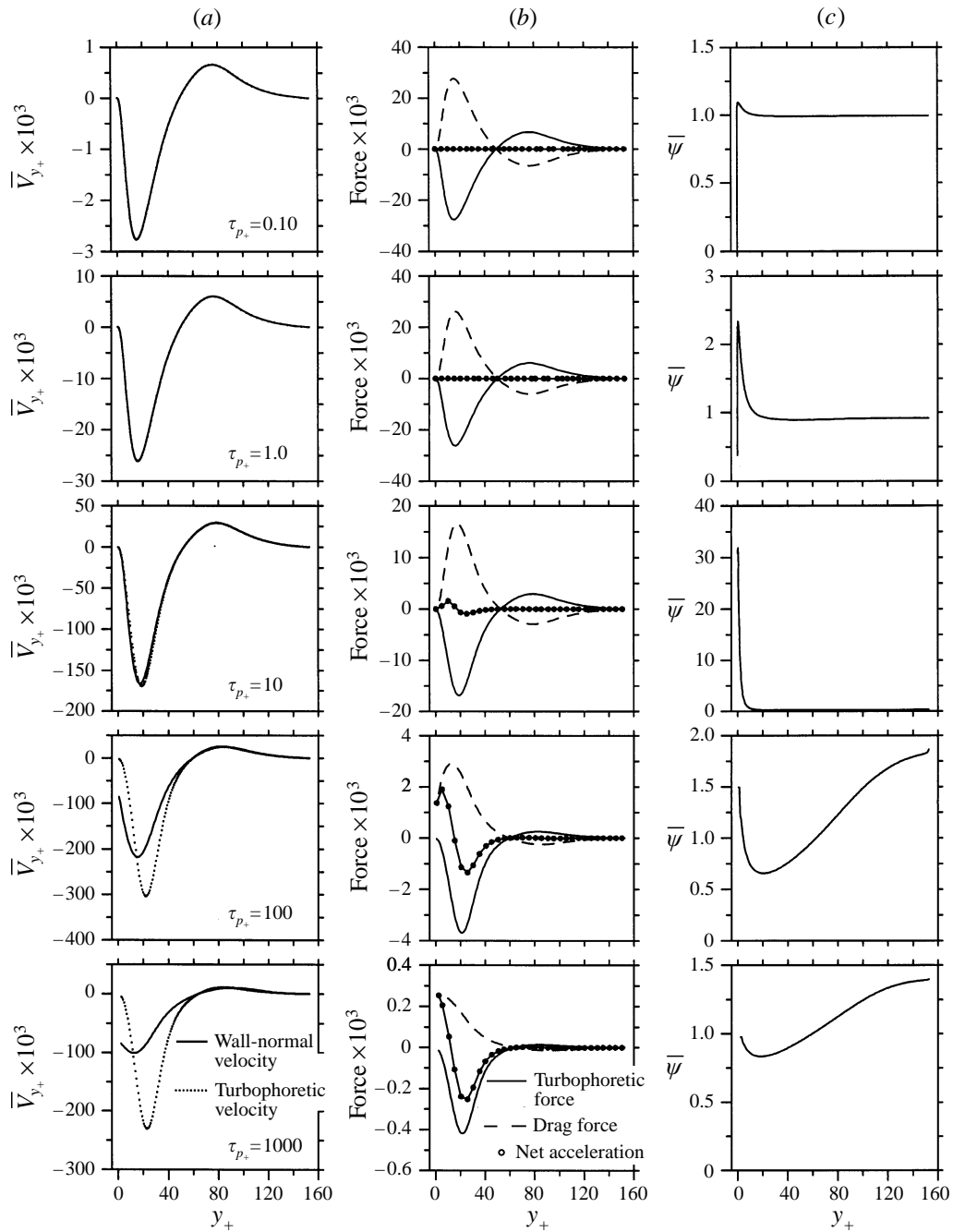
FIGURE 8. Particle dynamic behaviour *neglecting* the Saffman lift force: profiles of (*a*) wall-normal velocity, (*b*) forces (−ve towards the wall) and acceleration, and (*c*) particle density (all dimensionless).

12.1. *Dynamic behaviour neglecting the Saffman lift force*

The Saffman force provides the only coupling between the radial and axial momentum equations (through the axial slip velocity $\bar{U}_z - \bar{V}_z$) and, if it is neglected, the governing set of equations is reduced to the radial momentum equation (61) and the particle
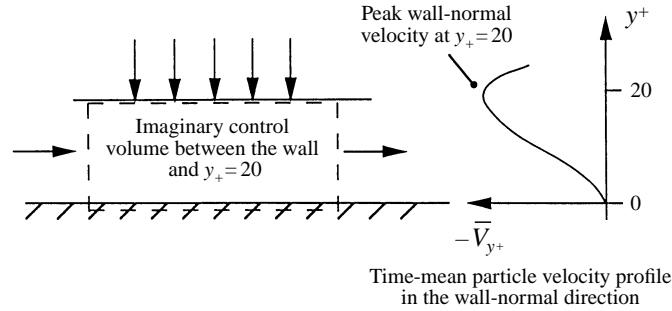
FIGURE 9. Particle fluxes in the near-wall region.

conservation equation (63). These are then sufficient to determine the (dimensionless) convective velocity field $\bar{V}_{y+}$ and the (dimensionless) particle density field $\bar{\psi}$.

Figure 8 shows profiles of $\bar{V}_{y+}$, acceleration and force per unit mass of particles, and $\bar{\psi}$ for $\tau_{p+} = 0.1$, 1, 10, 100 and 1000. Particles with $\tau_{p+} = 0.1$ are in the diffusional deposition regime, those with $\tau_{p+} = 1$, 10 and 100 represent the bottom, middle and top of the diffusion-impaction regime and those with $\tau_{p+} = 1000$ are situated well into the inertia-moderated regime.

Consider first the profiles of $\bar{V}_{y+}$ in figure 8(a), noting that negative values represent velocities directed towards the wall and that different ordinate scales have been used for the five diagrams. It is immediately obvious that all particle convective velocities are very small. The maximum wallwards velocity (for $\tau_{p+} = 100$) is about $0.2u_*$, whilst that for particles with $\tau_{p+} = 0.1$ is a mere $0.003u_*$. To put this in perspective, the axial velocity at the centre of the pipe is about $18u_*$.

The changing magnitude of $\bar{V}_{y+}$ with increasing τ_{p+} is closely related to the changing turbophoretic velocity $(\bar{V}_{y+})_{turbo}$, defined by (65). Figure 8(a) shows that profiles of $\bar{V}_{y+}$ and $(\bar{V}_{y+})_{turbo}$ are almost identical for the smaller particles ($\tau_{p+} < 10$) but display large differences for particles with greater inertia. Turbophoresis tends to accelerate particles down the turbulence gradient, the resultant viscous drag force attempting to restore them to a state of equilibrium with the gas. The inertia of particles with $\tau_{p+} < 10$ is sufficiently small for this balance to be struck and consequently, at the wall itself, the convective velocity is very small indeed. With increased inertia, the particles can 'coast' across the sub-layer and the convective velocity at the wall increases, a maximum value of $\bar{V}_{y+} \approx 0.1$ being attained at $\tau_{p+} \approx 100$. Further increase in τ_{p+} causes a gradual decline in the velocity at the wall due to the reduced response of the particles to the buffer layer turbulence. (The decline is gradual because, although larger particles respond less well to the turbulence, their increased inertia allows them to coast further.)

Figure 8(b) shows the corresponding force and acceleration profiles. All three terms of the radial momentum equation have been plotted in order to demonstrate graphically the changing relationships between turbophoresis, viscous drag and particle acceleration. The graphs also demonstrate that the level of artificial viscosity needed to stabilize the numerical integration has a negligible effect on the results. In the plots, the dots represent the particle acceleration, whilst the line through these dots is the net force per unit mass experienced by the particles minus the artificial dissipation term. Clearly, the two are indistinguishable.

It should now be clear that turbophoresis is the mechanism responsible for 'injecting' a convective flux of particles from the buffer layer into the region $y_+ < 20$, see figure 9. However, without a corresponding removal mechanism this would result in a continual accumulation of particles adjacent to the wall and a steady state could

never be achieved. Convection in the axial direction does not assist because the particle flow field is fully developed and hence the dimensionless axial particle flux for $y_+ < 20$ is independent of z. A mechanism must therefore exist for transporting particles to the wall at precisely the same rate as they enter from the buffer layer. Particles with large inertia can coast across the layer and then the radial flux in the region $y_+ < 20$ is purely convective with an approximately constant particle density. On the other hand, particles which cannot reach the wall by coasting rely on laminar or turbulent diffusional mechanisms to supplement the convective flux. The particle density profile therefore reflects the continuity requirement that the total radial particle flow, convective plus diffusive, must remain exactly constant in the region $y_+ < 20$.

Particle density profiles are shown in figure 8(c). The smallest particles ($\tau_{p+} = 0.1$) have only a tiny wallwards convective velocity and the particle density $\bar{\psi}$ is almost uniform except for a slight increase close to the wall. This spatial accumulation of particles serves to provide the steep gradient of $\bar{\psi}$ at the wall which is required to generate the necessary Brownian diffusional flux. As particle inertia increases ($\tau_{p+} = 1$) so too does the injected flux from the buffer region. The peak value of $\bar{\psi}$ then rises to establish the gradient necessary to sustain the increased diffusional flux at the wall. However, it can also be seen that $\bar{\psi}$ is non-zero at the wall itself. This implies that the flux of depositing particles has both a convective and a diffusive component.

By $\tau_{p+} = 10$, deposition is dominated by convection but, surprisingly, the peak value of $\bar{\psi}$, which occurs at the wall itself, is extremely large. However, this large increase in $\bar{\psi}$ is required, not to provide a gradient for diffusion (which actually tends to drive particles away from the wall), but to maintain a near-constant convective flux $\bar{\psi}\bar{V}_{y+}$, $\bar{V}_{y+}$ being very small indeed at the wall. With further increase in τ_{p+}, $\bar{V}_{y+}$ at the wall increases rapidly and a large peak value of $\bar{\psi}$ is no longer necessary to sustain the convective flux. Instead, a gradient of particle density develops in the central region of the pipe. This exactly counteracts, by diffusion, the tendency of turbophoresis in the core region to transport particles towards the centreline (discussed previously in connection with figure 2).

12.2. *Dynamic behaviour including the Saffman lift force*

Inclusion of the Saffman force couples the axial and radial momentum equations and the particle axial velocity profile can no longer be neglected. It is shown in figure 10(a), together with profiles of wall-normal velocity (figure 10b), force and acceleration (figure 10c) and particle density (figure 10d) for $\tau_{p+} = 1$, 10 and 100. To aid interpretation, profiles of $\bar{V}_{y+}$ and $\bar{\psi}$ for the case of no lift have also been included.

The response of particles with $\tau_{p+} \leqslant 1$ is unchanged by the addition of the lift force because the axial slip velocity is everywhere very small. With increasing inertia, however, particles transported towards the wall by turbophoresis 'retain a memory' of their own (higher) axial velocity from the core region. The resulting axial slip velocity (the particles now lead the fluid), occurring as it does in a strong shear flow, creates a wallwards force thus boosting the particle acceleration (see figure 10c).

Figure 10(b) shows that the effect on the wall-normal velocity of the larger particles is dramatic. Without lift, particles with $\tau_{p+} = 10$ have only a small convective velocity at the wall. With lift, the velocity increases by a factor of 20 to $\bar{V}_{y+} \approx 0.05$. In consequence, the enormous peak in particle density (30 times the bulk mean value, see figure 8c) is greatly reduced to around twice the mean, see figure 10(d). For particles with $\tau_{p+} \geqslant 100$, the lift force totally dominates the near-wall behaviour and the particles maintain their velocity all the way to the wall, the particle density therefore remaining approximately constant.
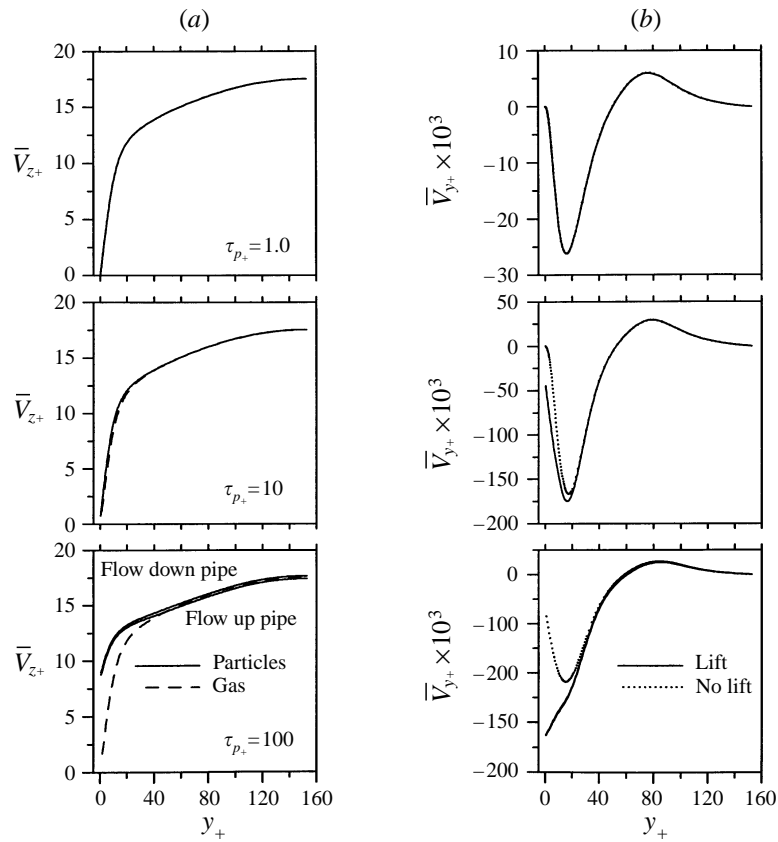
FIGURE 10(*a, b*). For caption see facing page.

The changing importance of the various force and acceleration terms is illustrated in figure 10(*c*) (which should be compared with the corresponding diagrams in figure 8*b*). For the larger particles, turbophoresis acts to create the initial wallwards drift but thereafter it is the lift force that drives the particles to the wall. This, in turn, explains the differing shapes of the deposition curves in figure 7. The maximum deposition rate is attained by particles with smaller τ_{p+} when lift is acting because this force tends to enhance the effects of inertia. In doing so, the peak near-wall particle density found in the upper diffusion-impaction regime is reduced since particles are better able to traverse the viscous sub-layer. This is illustrated in figure 11 which shows the peak value of $\bar{\psi}$ for both the lift and no-lift cases.

12.3. *The effect of gravity*

Calculations indicate that the effect of gravity on deposition rates from vertical flow is insignificant. Upward, as opposed to downward, flow in a pipe can easily be simulated by reversing the sign of g_+ in (62) but this has virtually no effect on the deposition rates. It is true that gravity creates a downwards drift velocity and hence the axial velocity profiles for particles flowing up and down the pipe are slightly different. However, the dominant reason for particle axial slip (and thence the generation of a lift force) is not this steady drift velocity but the rapid change in gas axial velocity as it is brought to rest at the wall. In contrast, the calculations of Johansen (1991) indicated that gravity does play a significant role in deposition from vertical flows. Unfortunately, because
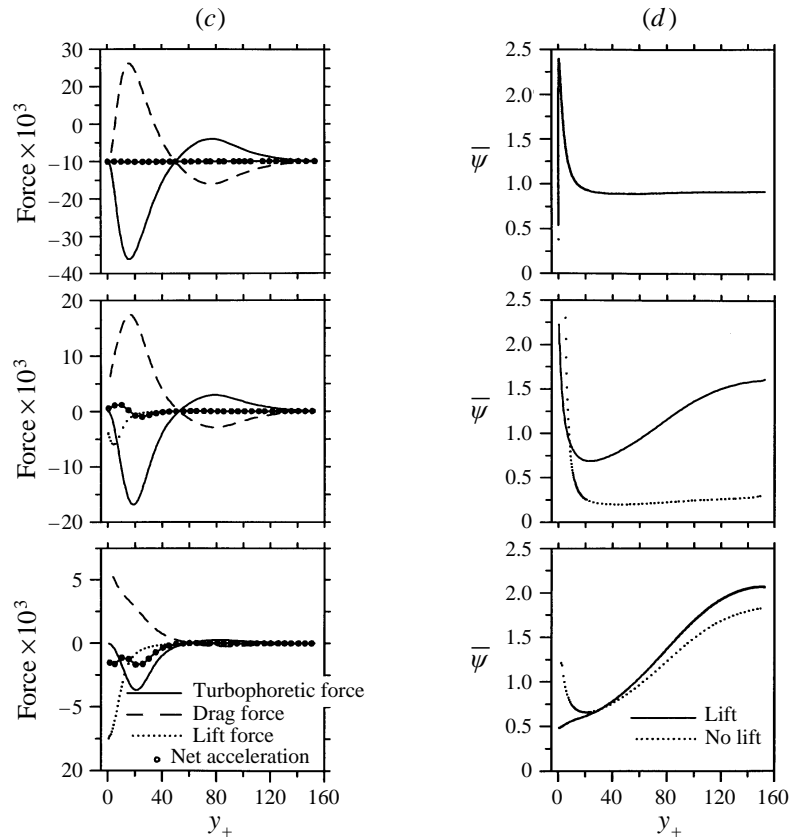
FIGURE 10. Particle dynamic behaviour *including* the Saffman lift force: profiles of (*a*) axial velocity, (*b*) wall-normal velocity, (*c*) forces (−ve towards the wall) and acceleration, and (*d*) particle density (all dimensionless).
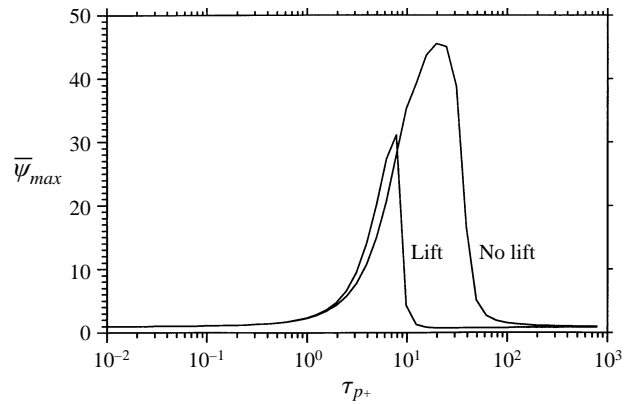
FIGURE 11. The effect of the Saffman lift force on the variation with τ_{p+} of the peak (dimensionless) particle density near the wall.
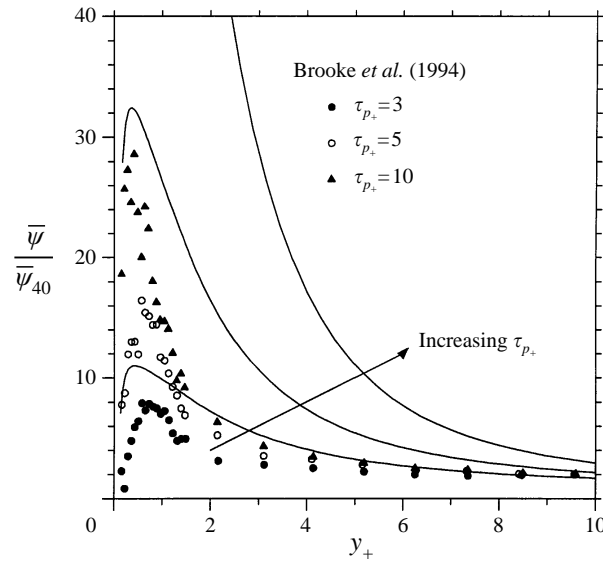
FIGURE 12. Particle density profiles near the wall: a comparison of the present theory with results from the direct numerical simulations of Brooke *et al.* (1994).

of the complexity of his turbulence modelling, it is difficult to pinpoint the cause of this disagreement.

12.4. *Validation*

One of the striking results of the deposition theory is the prediction of increased particle density close to the wall in the diffusion-impaction regime. This is not shown by any of the free-flight theories of deposition and provides an obvious possibility for experimental validation. At present, however, the only relevant published experiments are those of Sun & Lin (1986) who investigated a flow of polydispersed sodium chloride particles in air. Although their results are not quantifiable, they did report a 'preferential concentration' of particles near the wall which is, at least, encouraging.

Further corroboratory evidence can be obtained from direct numerical simulations. Figure 12 shows the variation of $\bar{\psi}$ (normalized by its value at $y_+ = 40$) in the region $y_+ < 10$ for three particle classes in the diffusion-impaction regime ($\tau_{p+} = 3$, 5 and 10). Included are predictions from the present model together with the DNS results of Brooke *et al.* (1994) (who did not include the Saffman force in their calculations). The present approach agrees well with the DNS data for $\tau_{p+} = 3$ but the peak particle density is overpredicted by some 50% for $\tau_{p+} = 5$ and by almost 100% for $\tau_{p+} = 10$.

The correct prediction of the particle density near the wall is a severe test of any transport model, either Eulerian or Lagrangian based, and it would be unwise to give too much credence to the curves of figure 12. Nevertheless, an excessive preferential concentration of mid-sized particles coupled with an underpredicted deposition velocity is an indication that the turbophoresis model may require further attention. The main deficiency of the present model is its failure to acknowledge the fact that the more massive particles retain a 'memory' of the turbulence level of the gas through which they have just passed. In consequence, the turbophoretic force associated with these particles would probably decay less rapidly near the wall than the simple model implies, thus resulting in a larger wall-normal velocity, an increase in deposition rate and a reduction in peak particle density.

The interplay between turbophoresis, viscous drag and Saffman lift near the wall is

evidently very complex and the balance illustrated in figure 10 may well be altered significantly by the addition of a 'turbulence memory' effect. Furthermore, as was noted earlier, wall-proximity effects on the particle lift and drag forces have been neglected in the analysis and these may also play a significant part. Nevertheless, the general conclusion that the Saffman lift force makes an important contribution, both to the rate of deposition and to the near-wall particle density profile in the upper diffusion-impaction and inertia-moderated regimes, appears justified. Further work is required, however, to define precisely the relative importance of each transport mechanism.

13. Conclusions

Unlike most previous theories, the deposition model presented in this paper is based formally on the conservation equations of particle mass and momentum. These equations are formulated in an Eulerian coordinate system and are Reynolds averaged. The averaging process generates a number of turbulence correlations of which two are of prime importance. One is the familiar turbulent diffusion flux, 'driven' by the time-mean particle density gradient. The other is turbophoresis, a convective drift of particles down gradients of mean-square fluctuating velocity. Turbophoresis is not a small correction: it dominates the particle dynamic behaviour in the diffusion-impaction and inertia-moderated regimes. Nonetheless, its importance has been recognized by very few of the many workers in this field.

Using a very simple model for the turbophoretic force, the theory has been used to calculate deposition from fully developed turbulent pipe flow. The particle conservation equations have been solved numerically and deposition rates calculated for a range of dimensionless relaxation times encompassing all the familiar deposition regimes ($10^{-2} \leqslant \tau_{p+} \leqslant 10^{+3}$). Agreement between calculations and measurements is very good apart from a tendency to underpredict deposition rates in the upper diffusion-impaction regime. In this region, the simple model of turbophoresis, related as it is to the local gas turbulence structure, may need to be extended to include the effects of particle 'memory'.

The relationship between the Saffman lift force, turbophoresis and viscous drag is complex and the balance may be significantly altered by the inclusion of a particle 'memory' effect in the turbophoresis model. Nevertheless, it is probable that the Saffman force plays an important role in the inertia-moderated regime. In contrast, the effect of gravity on deposition from vertical flows appears to be negligible.

Unlike previous free-flight theories, the model predicts an increase in particle density close to the wall in the diffusion-impaction regime. This result, which is partially corroborated by DNS calculations, provides a possibility for future experimental validation. However, the peak particle density is very sensitive to the details of the turbulence model and very precise measurements will be required if reliable conclusions are to be drawn.

The deposition theory presented in this paper represents a considerable advance in physical understanding over previous free-flight theories. It also offers many avenues for future development. For example, using essentially the same turbulence models, the theory can formally be extended to simulate three-dimensional particle transport in more complex gas flow fields thus allowing the simultaneous calculation of laminar (pure inertial) and turbulent particle transport using a universal numerical scheme (as opposed to the cumbersome mixed Lagrangian–Eulerian methods currently in use). Of course, such developments presuppose an accurate knowledge of the gas turbulence

field and the current limitations in fluid turbulence prediction methods may well provide the real restrictions to applications in particle transport problems. Nevertheless, the formalism is established and it is clear that the full-Eulerian Reynolds-averaged approach offers many advantages for physical interpretation and practical calculation which are not possible with other methods.

Appendix A. Boundary condition at the pipe wall

The assumption that the particles are in local equilibrium with the turbulence everywhere in the pipe implies that, when they enter the sub-layer, they do not carry with them the random motion generated by the turbulence through which they have just passed. Nevertheless, it is incorrect to assert that, at the 'wall', the only *diffusive* process operating is that due to Brownian motion. The 'wall' boundary condition is actually applied one particle radius distance from the solid surface because particles can then deposit by interception. At this point, the turbulence has not quite decayed to zero and eddy diffusion may still be a significant transport mechanism if the laminar Schmidt number is large.

Consider an imaginary interface a very short distance λ from the pipe wall (see figure 13). At the interface, the particle mass flux towards the wall J is

$$J = \bar{\rho}_p \bar{V}_r - (D_p + D_{turb}) \frac{\partial \bar{\rho}_p}{\partial r}. \tag{A 1}$$

It is now assumed that the particles possess a Maxwellian distribution of velocities centred around the convective velocity $\bar{V}_r$. Let $f(\xi_r, \xi_\phi, \xi_z) \, d\xi_r \, d\xi_\phi \, d\xi_z$ be the number of particles per unit volume having components of velocity in the range $\xi_r \to \xi_r + d\xi_r$, $\xi_\phi \to \xi_\phi + d\xi_\phi$, $\xi_z \to \xi_z + d\xi_z$. The mass flux of particles directed towards the wall is thus

$$J = \int_{-\infty}^{\infty} \int_{-\infty}^{\infty} \int_{0}^{\infty} m_p \xi_r f(\xi_r, \xi_\phi, \xi_z) \, d\xi_r \, d\xi_\phi \, d\xi_z. \tag{A 2}$$

The integral is best performed by defining

$$c_r = \frac{\xi_r - \bar{V}_r}{(2R_p T)^{1/2}}, \quad c_\phi = \frac{\xi_\phi}{(2R_p T)^{1/2}}, \quad c_z = \frac{\xi_z - \bar{V}_z}{(2R_p T)^{1/2}},$$

where $R_p = k/m_p$. The distribution function in terms of (c_r, c_ϕ, c_z) is then

$$f(c_r, c_\phi, c_z) = n_p (2\pi R_p T)^{-3/2} \exp[-(c_r^2 + c_\phi^2 + c_z^2)]. \tag{A 3}$$

Transforming the variables and performing the integrations using standard results gives

$$J = \tfrac{1}{2} m_p n_p \bar{V}_r \left[1 + \mathrm{erf}(M_r) + \frac{1}{\pi^{1/2} M_r} \exp(-M_r^2) \right], \tag{A 4}$$
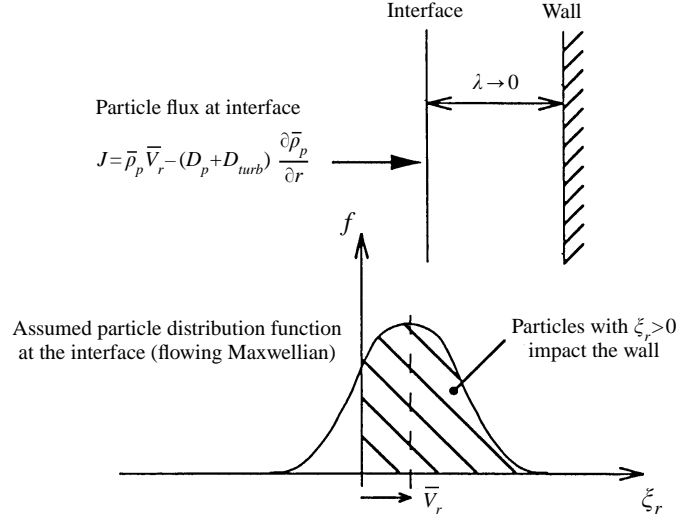
FIGURE 13. The wall boundary condition: particle fluxes very near the solid surface.

where $M_r = \bar{V}_r/(2R_p T)^{1/2}$ and erf is the error function. Assuming λ to be small so that (A 1) and (A 4) are effectively evaluated at the same position gives

$$J_w = \left[\bar{\rho}_p \bar{V}_r - (D_p + D_{turb}) \frac{\partial \bar{\rho}_p}{\partial r} \right]_w$$

$$= \left[\tfrac{1}{2} \bar{\rho}_p \bar{V}_r \left(1 + \text{erf}(M_r) + \frac{1}{\pi^{1/2} M_r} \exp\left(-M_r^2\right) \right) \right]_w. \tag{A 5}$$

If $\bar{V}_{rw}$ is known from the solution of the momentum equation, (A 5) provides a relationship between $\bar{\rho}_{pw}$ and $(\partial \bar{\rho}_p/\partial r)_w$.

Appendix B. Turbulence models for the gas flow field

The model for the eddy viscosity ν_{turb} is a modified version of that proposed by Granville (1990). It is a two-layer model, the eddy viscosity being described by separate functions for the near-wall and core flows, blended by a smooth transition. In dimensionless form

$$\nu_{turb}/\nu_g = \nu_{c+} \tanh\left(\nu_{w+}/\nu_{c+}\right). \tag{B 1}$$

In the near-wall region

$$\nu_{w+} = \kappa y_+ [1 - \exp\left(y_+^2/\lambda_+^2\right)], \tag{B 2}$$

where $y_+ = yu_*/\nu_g$, $\kappa = 0.40$ is von Kármán's constant and $\lambda_+ = 24$. As explained elegantly by Chapman & Kuhn (1986), the eddy viscosity should vary with y^3 very near the wall and the model predicts this behaviour correctly ($\nu_{w+} \simeq \kappa y_+^3/\lambda_+^2$). It also recovers the so-called 'law of the wall' in the logarithmic region of the flow. For the core flow,

$$\nu_{c+} = \nu_{o+} \left[1.1 - \frac{0.2}{\pi} \arctan\left(\frac{y_+^2}{(a_+ - y_+)^2} \right) \right], \tag{B 3}$$

where ν_{o+} represents the velocity defect model of Cebeci & Smith (1974),

$$\nu_{o+} = \alpha \bar{U}_{zo+} \delta_+, \quad \delta_+ = \int_0^{a_+} \left(\frac{r_+}{a_+} \right) \left(1 - \frac{\bar{U}_{z+}}{\bar{U}_{zo+}} \right) dr_+. \tag{B 4}$$

$\bar{U}_{zo+}$ is the dimensionless time-mean velocity at the pipe centreline and $\alpha = 0.03$ as suggested by Nituch, Sjolander & Head (1978). The correction to ν_{o+} embodied in (B 3) ensures that the eddy viscosity reaches a maximum at $y_+ \simeq 40$ which is some 10% greater than the value at the pipe centreline.

The model adopted for the radial component of the mean-square fluctuating velocity $(\overline{u'_{y+} u'_{y+}})$ is similar in form to that used for the eddy viscosity. Thus

$$(\overline{u'_{y+} u'_{y+}})^{1/2} = u_{c+} \tanh(u_{w+}/u_{c+}), \tag{B 5}$$

where

$$u_{w+} = 0.0373 y_+ [1 - \exp(-y_+/4.67)], \tag{B 6}$$

$$u_{c+} = 0.90 - \frac{0.54}{\pi} \arctan\left(\frac{y_+^2}{(a_+ - y_+)^2}\right). \tag{B 7}$$

The constants were chosen to satisfy various boundary values and limiting behaviour as suggested by the direct numerical simulations of Kim *et al.* (1987). The model was designed for a Reynolds number of 4000 and no modifications were included to reflect the changing behaviour of the core flow at higher Reynolds numbers. This should have little effect on the prediction of deposition rates, however, as these are mainly controlled by the turbulence variations close to the wall.

REFERENCES

BEAL, S. K. 1970 Deposition of particles in turbulent flow on channel or pipe walls. *Nucl. Sci. Engng* **40**, 1–11.

BROOKE, J. W., HANRATTY, T. J. & MCLAUGHLIN, J. B. 1994 Free-flight mixing and deposition of aerosols. *Phys. Fluids* **6**, 3404–3415.

CEBECI, T. & SMITH, A. M. O. 1974 *Analysis of Turbulent Boundary Layers*, p. 171. Academic Press.

CHAPMAN, D. R. & KUHN, G. D. 1986 The limiting behaviour of turbulence near a wall. *J. Fluid Mech.* **170**, 265–292.

CUNNINGHAM, E. 1910 On the velocity of steady fall of spherical particles through fluid medium. *Proc. R. Soc. Lond.* A **83**, 357–365.

DAVIES, C. N. 1966 Deposition from moving aerosols. In *Aerosol Science* (ed. C. N. Davies), pp. 393–446. Academic Press.

ECKELMANN, H. 1974 The structure of the viscous sublayer and the adjacent wall region in a turbulent channel flow. *J. Fluid Mech.* **65**, 439–459.

FERNANDEZ DE LA MORA, J. F. & ROSNER, D. E. 1982 Effects of inertia on the diffusional deposition of small particles to spheres and cylinders at low Reynolds numbers. *J. Fluid Mech.* **125**, 379–395.

FISCHER, T. M. & ROSENBERGER, R. 1987 A boundary integral method for the numerical computation of the forces exerted on a sphere in viscous incompressible flows near a plane wall. *Z. Angew. Math. Phys.* **38**, 339–365.

FRIEDLANDER, S. K. & JOHNSTONE, H. F. 1957 Deposition of suspended particles from turbulent gas streams. *Ind. Engng Chem.* **49**, 1151–1156.

GRANVILLE, P. S. 1990 A near-wall eddy viscosity formula for turbulent boundary layers in pressure gradients suitable for momentum, heat, or mass transfer. *Trans. ASME: J. Fluids Engng* **112**, 240–243.

HINZE, J. O. 1975 *Turbulence*, 2nd Edn. McGraw-Hill.

JOHANSEN, S. T. 1991 The deposition of particles on vertical walls. *Intl J. Multiphase Flow* **17**, 355–376.

KALLIO, G. A. & REEKS, M. W. 1989 A numerical simulation of particle deposition in turbulent boundary layers. *Intl J. Multiphase Flow* **15**, 443–446.

KIM, J., MOIN, P. & MOSER, R. 1987 Turbulence statistics in fully developed channel flow. *J. Fluid Mech.* **177**, 136–166.

LAUFER, J. 1954 Structure of turbulence in fully developed pipe flow. *NACA Rep.* 1174.

LEE, M. M., HANRATTY, T. J. & ADRIAN, R. J. 1989 The interpretation of droplet deposition measurements with a diffusion model. *Intl J. Multiphase Flow* **15**, 459–469.

LEEMING, A. D. 1996 Particle deposition from turbulent flows. PhD thesis, Cambridge University Engineering Department.

LIU, B. Y. H. & AGARWAL, J. K. 1974 Experimental observation of aerosol deposition in turbulent flow. *Aerosol Sci.* **5**, 145–155.

LIU, B. Y. H. & ILORI, T. Y. 1974 Aerosol deposition in turbulent pipe flow. *Environ. Sci. Technol.* **8**, 351–356.

MAXEY, M. R. & RILEY, J. J. 1983 Equation of motion for a small rigid sphere in a nonuniform flow. *Phys. Fluids* **26**, 883–889.

MCLAUGHLIN, J. B. 1993 The lift on a small sphere in wall-bounded linear shear flows. *J. Fluid Mech.* **246**, 249–265.

MEI, R. 1992 An approximate expression for the shear lift force on a spherical particle at finite Reynolds number. *Intl J. Multiphase Flow* **18**, 145–147.

MORSI, S. A. & ALEXANDER, A. J. 1972 An investigation of particle trajectories in two-phase flow systems. *J. Fluid Mech.* **55**, 193–208.

NITUCH, M. J., SJOLANDER, S. & HEAD, M. R. 1978 An improved version of the Cebeci-Smith eddy-viscosity model. *Aeronaut. Q.* **29**, 207–225.

NUNNER, W. 1956 Wärmeübergang und Druckabfall in rauhen Rohren. *VDI Forschungsheft* 455.

PAPERVERGOS, P. G. & HEDLEY, A. B. 1984 Particle deposition from turbulent flows. *Chem. Engng Res. Des.* **62**, 275–295.

PICART, A., BERLEMONT, A. & GOUESBET, B. 1986 Modelling and predicting turbulence fields and the dispersion of discrete particles transported by turbulent flows. *Intl J. Multiphase Flow* **12**, 237–261.

PISMEN, L. M. & NIR, A. 1978 On the motion of suspended particles in stationary homogeneous turbulence. *J. Fluid Mech.* **84**, 193–206.

RAMSHAW, J. D. 1979 Brownian motion in a flowing fluid. *Phys. Fluids* **22**, 1595–1601.

RAMSHAW, J. D. 1981 Brownian motion in a flowing fluid revisited. *Phys. Fluids* **24**, 1210–1211.

REEKS, M. W. 1977 On the dispersion of small particles suspended in an isotropic turbulent fluid. *J. Fluid Mech.* **83**, 529–546.

REEKS, M. W. 1983 The transport of discrete particles in inhomogeneous turbulence. *J. Aerosol Sci.* **14**, 729–739.

REEKS, M. W. 1993 On the constitutive relations for dispersed particles in nonuniform flows. I. Dispersion in a simple shear flow. *Phys. Fluids* A **5**, 750–761.

SCHWENDIMAN, L. C. & POSTMA, A. K. 1962 Turbulent deposition in sampling lines. *Tech. Inf. Div. Rep.* TID-7628, Book 1, (USAEC).

SEHMEL, G. A. 1968 Aerosol deposition from turbulent airstreams in vertical conduits. *Batelle Northwest Lab., Richland, Washington, USA, Rep.* BNWL-578.

SUN, Y. F. & LIN, S. P. 1986 Aerosol concentration in a turbulent flow. *J. Colloid Interface Sci.* **113**, 315–320.

WELLS, A. C. & CHAMBERLAIN, A. C. 1967 Transport of small particles to vertical surfaces. *Brit. J. Appl. Phys.* **18**, 1793–1799.